Published in final edited form as:
Sci Transl Med. 2024 January 10; 16(729): eadh1334. doi:10.1126/scitranslmed.adh1334.

mRNA therapy corrects defective glutathione metabolism and restores ureagenesis in preclinical argininosuccinic aciduria

Sonam Gurung[1,*], **Oskar Vilhelmsson Timmermand**[2,*], **Dany Perocheau**[1,*], **Ana Luisa Gil-Martinez**[1], **Magdalena Minnion**[3,4], **Loukia Touramanidou**[1], **Sherry Fang**[5], **Martina Messina**[5], **Youssef Khalil**[1], **Justyna Spiewak**[1], **Abigail R. Barber**[2], **Richard S. Edwards**[2], **Patricia Lipari Pinto**[6], **Patrick F. Finn**[7], **Alex Cavedon**[7], **Summar Siddiqui**[7], **Lisa Rice**[7], **Paolo G.V. Martini**[7], **Deborah Ridout**[1], **Wendy Heywood**[1], **Ian Hargreaves**[8], **Simon Heales**[1,5], **Philippa B. Mills**[1], **Simon N. Waddington**[9,10], **Paul Gissen**[1,5,11], **Simon Eaton**[1], **Mina Ryten**[1], **Martin Feelisch**[3,4], **Andrea Frassetto**[7], **Timothy H. Witney**[2,ǂ], **Julien Baruteau**[1,5,11,ǂ]

[1]Great Ormond Street Institute of Child Health, University College London, London WC1N 1EH, UK

[2]School of Biomedical Engineering and Imaging Sciences, King's College London, London SE1 7EH, UK

[3]Clinical and Experimental Sciences, Faculty of Medicine, University of Southampton, Southampton SO17 1BJ, UK

[4]Southampton NIHR Biomedical Research Centre, University Hospital Southampton NHS Foundation Trust, UK

[5]Great Ormond Street Hospital for Children NHS Foundation Trust, London, Southampton SO16 6YD, UK

[6]Santa Maria's Hospital, Lisbon North University Hospital Center, 1649-028 Lisbon, Portugal

[7]Moderna Inc., Cambridge, MA 02139, USA

[8]Pharmacy and Biomolecular Sciences, Liverpool John Moore University, Liverpool L3 5UG, UK

[9]EGA Institute for Women's Health, University College London, London WC1E 6HX, UK

Correspondence to: Julien Baruteau.

Corresponding author. j.baruteau@ucl.ac.uk.
*Shared first authorship
ǂShared senior authorship

Author Contributions: JB and THW designed the study. SG, OVT and DP conducted most of the experimental work. LT, YK, ARB, RSE, PBM, SNW and PG contributed to technical assistance in experimental work. ALGM and MR analysed the transcriptomics data. MM and MF analysed the thiol reactome data. SF and MM collected patients' data. SE analysed the ureagenesis with stable isotope. PFF, AC, SS, LR, PGVM, AF provided the *Luc* and *hASL* mRNA constructs. SG wrote the manuscript. DR provided assistance with statistical analysis. All authors contributed to review/editing and approved the final submission.

Competing interests: JB reports research funding from Moderna Inc. JB, LT, DP, PG and SNW are inventors of patent application no PCT/GB2023/052174 "Gene therapy transgene cassette for the treatment of argininosuccinate lyase deficiency". PFF, AC, SS, LR, PGVM, AF are employees of Moderna Inc. and may hold equities from the company. AF and LR are inventors of patent application no. PCT/US23/17573 "Lipid nanoparticles and polynucleotides encoding arginosuccinate lyase for the treatment of argininosuccinic aciduria". The other authors declare no competing interests.

[10]Wits/SAMRC Antiviral Gene Therapy Research Unit, Faculty of Health Sciences, University of Witswatersrand, Braamfontein 2000, Johannesburg, South Africa

[11]National Institute of Health Research Great Ormond Street Biomedical Research Centre, London WC1N 1EH, UK

Abstract

The urea cycle enzyme argininosuccinate lyase (ASL) enables the clearance of neurotoxic ammonia and the biosynthesis of arginine. Patients with ASL deficiency present with argininosuccinic aciduria, an inherited metabolic disease with hyperammonaemia and a systemic phenotype coinciding with neurocognitive impairment and chronic liver disease. Here, we describe the dysregulation of glutathione biosynthesis and upstream cysteine utilization in ASL-deficient patients and mice using targeted metabolomics and *in vivo* positron emission tomography (PET) imaging using (*S*)-4-(3-^{18}F-fluoropropyl)-L-glutamate ([^{18}F]FSPG). Upregulation of cysteine metabolism contrasted with glutathione depletion and down-regulated antioxidant pathways. To assess hepatic glutathione dysregulation and liver disease, we present [^{18}F]FSPG PET as a non-invasive diagnostic tool to monitor therapeutic response in argininosuccinic aciduria. Human *hASL* mRNA encapsulated in lipid nanoparticles improved glutathione metabolism and chronic liver disease. In addition, *hASL* mRNA therapy corrected and rescued the neonatal and adult Asl-deficient mouse phenotypes, respectively, enhancing ureagenesis. These findings provide mechanistic insights in liver glutathione metabolism and support clinical translation of mRNA therapy for argininosuccinic aciduria.

Introduction

Urea cycle defects (UCDs) are inborn errors of metabolism that cause dysfunction in ammonia detoxification and endogenous arginine synthesis. Argininosuccinic aciduria (ASA) (OMIM 207900) is the second most common UCD, occurring ~1 in every 100,000 live births (1). ASA is caused by deficiency in argininosuccinate lyase (ASL), a cytosolic urea cycle enzyme, which catalyses the conversion of argininosuccinate into arginine and fumarate, thereby enabling the removal of excess nitrogen (2, 3). ASL is also involved in the citrulline-nitric oxide (NO) cycle to produce NO through the channelling of extracellular L-arginine to nitric oxide synthase (NOS) (4, 5).

Patients with ASA display acute hyperammonaemia and a chronic phenotype of neurocognitive impairment and liver disease (3). The aims of the current therapeutic guidelines for ASA are to normalise ammonia and arginine concentrations through a low-protein diet, ammonia scavenging drugs, and arginine supplementation. Liver transplantation is used in cases of progressive liver disease or recurrent hyperammonaemic crises that occur despite conventional treatment. Proposed experimental treatments include antioxidants, autophagy enhancers, creatinine supplementation, and gene therapies (2, 6–12).

Chronic liver dysfunction causes morbidity in all UCD subtypes (13, 14) but is reported with higher frequency and severity in ASA (1, 11, 13, 15). This liver disease commonly manifests with hepatomegaly and transaminitis and can progress to liver failure and, eventually, hepatocellular carcinoma (11, 14–19). Liver pathology progresses despite appropriate

ammonia control, suggesting hyperammonaemia is not the sole cause (14). Other suggested mechanisms include arginine deficiency, argininosuccinate toxicity, NO deficiency, and oxidative stress (15, 16, 20). There are no reliable biomarkers that predict the degree of liver disease in ASA (16) and the underlying processes that trigger liver disease are unclear. More detailed mechanistic insight into liver pathophysiology will be crucial to identifying optimal diagnostic markers for better assessment of disease severity, prediction of disease progression, and assessment of response to therapy.

The *Asl*$^{Neo/Neo}$ mouse model recapitulates much of human ASA, with reports of hepatomegaly, elevated transaminases, aberrant hepatic glycogen accumulation, and variable fibrosis (2, 6, 9, 11, 12). Here, we studied the dysregulation of liver glutathione metabolism and its role in the chronic liver disease observed in both patients with ASA and *Asl*$^{Neo/Neo}$ mice. We assessed pathways of glutathione biosynthesis, which requires the rate-limiting biosynthetic enzyme glutamate cysteine ligase (GCL), glutathione recycling with γ-glutamyltranspeptidase (GGT) activity and metabolic fluxes through the hepatic antiporter system x_c^-, which promotes glutathione synthesis to counteract oxidative stress in health and disease (21). System x_c^- activity was monitored with the positron emission tomography (PET) radiotracer (*S*)-4-(3-^{18}F-fluoropropyl)-L-glutamate ([^{18}F]FSPG) used both as a diagnostic tool and to assess the progression of liver disease in ASA. mRNA therapy was tested as a treatment for both neonatal and adult *Asl*$^{Neo/Neo}$ mice to restore both glutathione metabolism and ureagenesis *in vivo*.

Results

ASL-deficient patients and *Asl*$^{Neo/Neo}$ mice show downregulation of glutathione biosynthesis despite limited evidence of oxidative stress

Compared to other UCDs, previous publications have highlighted the role of oxidative stress in the pathophysiology of ASL deficiency (5, 9, 22). To better understand the cellular response to this oxidative stress, we explored the role of glutathione, the body's primary antioxidant, and its regulation in ASA including its close interaction with the transsulfuration pathway (Figure 1A). We compared the plasma concentrations of total homocysteine, glycine, and glutamate in patients from Great Ormond Street Hospital for Children, London, UK who were affected by one of the 3 main urea cycle defects: ornithine transcarbamylase deficiency (OTCD; n=10), argininosuccinate synthase deficiency (ASSD; n=10), or argininosuccinate lyase deficiency (ASLD; n=13). Two liver-transplanted patients with OTCD were excluded due to normalised ureagenesis. Compared to OTCD and ASSD, patients with ASLD had significantly higher mean plasma concentrations of metabolites contributing to glutathione biosynthesis: homocysteine (Figure 1B) and glycine (Figure S1A). Plasma concentrations of glutamate, another precursor metabolite of glutathione, was not increased (Figure S1B). Plasma total homocysteine did not differ between early- and late-onset ASA (Figure S1C). Since follow-up, total plasma homocysteine (Figure S1D), glycine (Figure S1E) and glutamate (Figure S1F) concentrations remained significantly elevated for all patients with ASLD compared to those with OTCD and ASSD.

No sex difference was observed for plasma homocysteine and glycine (Table S1). Glutamate concentrations, however, were significantly elevated in females with OTCD and ASLD

compared to males (Table S1). Glutamate and glycine plasma concentrations are easily influenced by diet, medications, metabolic control, and delayed analytical processing. Clinical information regarding these patients with OTCD, ASSD, and ASLD are presented in Table S2. Samples collected during hyperammonemic episodes were excluded from data collection. Patients with average total homocysteine above the normal upper range limit were not screened for methyltetrahydrofolate (*MTHFR*) polymorphism, which may contribute to the differences observed here between patient types. No vitamin B12 deficiency was observed in the patients (Figure S1G).

We measured the metabolites of the glutathione pathway in the hypomorphic $Asl^{Neo/Neo}$ mouse model, which recapitulates much of the human phenotype of ASLD (4, 9). As sulfur-containing amino acids (and H_2S) exist in different forms (23), we measured both total and reduced free thiol form (R-SH) to determine any compromise to the cellular antioxidant buffering capacity. Corroborating human data, plasma total (Figure 1C) and free (Figure S2A) homocysteine concentrations in 2-week-old $Asl^{Neo/Neo}$ mice were significantly elevated compared to WT littermates. Other plasma metabolites of the glutathione biosynthesis pathway, total (Figure 1D) and free (Figure S2B) cysteine were also significantly increased in $Asl^{Neo/Neo}$ mice compared to WT. Total γ-glutamyl-cysteine (Figure 1E) and free γ-glutamyl-cysteine (Figure S2C) showed no difference. In contrast, plasma total glutathione was significantly decreased (Figure 1F). Most of the glutathione released in the bloodstream is synthesised in the liver (24). Similar to plasma, liver concentrations of total (Figure 1G) and free (Figure S2D) homocysteine, total (Figure 1H) and free (Figure S2E) cysteine, and total γ-glutamyl-cysteine (Figure 1I) showed a significant increase in $Asl^{Neo/Neo}$ mice compared to WT. Liver free γ-glutamyl-cysteine (Figure S2F) showed no difference. As in plasma, total glutathione concentrations in liver were significantly decreased but to a far greater extent (Figure 1J).

Total glutathione is degraded by GGT at the external surface of epithelial cells (25). GGT activity and expression in liver showed a significant 5-fold increase in $Asl^{Neo/Neo}$ mice compared to WT (Figure 1K and Figure S2G). Total cysteine-glycine synthesised from glutathione catabolism by GGT was also increased in liver (Figure S2H), although free cysteine-glycine was unchanged (Figure S2I). $Asl^{Neo/Neo}$ mice (4) and patients with ASA (26, 27) may present chronic kidney disease and renal failure. Supporting this, urine glutathione concentrations were significantly increased in $Asl^{Neo/Neo}$ mice compared to WT, suggesting defective renal glutathione reabsorption (Figure S2J). Urine cysteine concentrations were also significantly increased in $Asl^{Neo/Neo}$ mice compared to WT (Figures S2K), in line with an elevation of these metabolites in the plasma and livers, a consequence which is partially explained by increased GGT activity. Urine cysteine-glycine concentrations, however, were not significantly increased (Figure S2L).

The increase of free thiols metabolites suggested that the persisting buffering capacity and protective role against oxidative stress of free thiols (23, 28) was maintained both systemically and in the liver. To better characterise the oxidative stress in ASA, we assessed the ratio of reduced (GSH) versus oxidised glutathione (GSSG), whereby a reduction in this ratio is a common marker of oxidative stress (29). Here the liver GSH:GSSG ratio did not differ between $Asl^{Neo/Neo}$ and WT littermates (Figure S2M), indicating that the reduction

of total glutathione pool in *Asl*$^{Neo/Neo}$ mice was not associated with increased glutathione oxidation. The comparison of the different steady-state concentrations of the precursors and breakdown products of glutathione suggested that precursors accumulated due to a bottleneck in one of the rate-limiting steps of glutathione biosynthesis, whereas glutathione catabolism by GGT was enhanced, explaining the lower glutathione concentrations in both the circulation and in the liver of *Asl*$^{Neo/Neo}$ mice.

To determine whether oxidative stress might further contribute to the lower concentrations of total glutathione in plasma and liver of *Asl*$^{Neo/Neo}$ mice, we measured lipid peroxidation products in the liver using the thiobarbituric acid reactive substances (TBARS) assay. Lipid peroxidation was not significantly increased in *Asl*$^{Neo/Neo}$ mice versus WT (Figure 1L). The steady-state concentration of the oxidative breakdown products of NO, nitrite (NO_2^-) and nitrate (NO_3^-), were significantly lower in plasma (Figure S2N) and liver (Figure 1M), as previously reported in this disorder (4, 5). Nitroso-species showed no difference between *Asl*$^{Neo/Neo}$ livers versus WT, and did not support NO deficiency as a critical pathophysiological mechanism in the liver (Figure S2O). The lack of difference in nitrotyrosine concentrations by western blot in *Asl*$^{Neo/Neo}$ livers versus WT confirmed the absence of nitro-oxidative stress (Figure 1N, Figure S2P). The nuclear factor erythroid 2-related factor 2 (Nrf2) is a transcriptional factor regulating antioxidant response against oxidative stress. Nrf2 protein abundances did not differ between WT and *Asl*$^{Neo/Neo}$ livers (Figure S2Q). Taken together, upstream precursors of glutathione biosynthesis accumulated in ASA, coinciding with reduced total glutathione, compromised NO production, moderate oxidative stress, and persisting antioxidant capacity.

Glutathione biosynthesis relies on 2 enzymatic steps: the rate limiting glutamate cysteine ligase (GCL) catalyses the conversion of glutamate and cysteine to γ-glutamyl-cysteine, and then glutathione synthase (GS) catalyses the conversion of γ-glutamyl-cysteine and glycine to glutathione. GCL is a heterodimer with a heavy catalytic subunit (GCLC) and a light or modifier subunit (GCLM) (25). We hypothesised that reduced glutathione was not a consequence of increased oxidative stress, but an effect of deficiencies in the enzymes involved in its biosynthesis. Indeed, *Asl*$^{Neo/Neo}$ mice had decreased gene expression of GCLC (Figure 1O) and GCLM (Figure 1P) compared to WT, whereas GS expression showed no significant difference (Figure 1Q). Supporting this, untargeted proteomics comparing WT and *Asl*$^{Neo/Neo}$ livers highlighted glutathione function as downregulated (Figure 1R, Figure S3A-C).

A non-invasive marker confirms impaired glutathione metabolism in *Asl*$^{Neo/Neo}$ mice

The biosynthesis of glutathione is dependent on cellular import of cystine in exchange for glutamate efflux via the cystine/glutamate antiporter system x_c^-, a transmembrane transport system (Figure 2A) (31). Cystine is subsequently reduced to cysteine for *de novo* glutathione biosynthesis (25). Metabolic reprogramming in cancer cells generate oxidative stress, which is balanced by increased glutathione biosynthesis via enhanced x_c^- mediated cystine import (30). Using positron emission tomography (PET), the radiolabelled glutamate analogue [^{18}F]FSPG provides an *in vivo* functional readout of *de novo* glutathione biosynthesis and

has been used both in the clinic for cancer diagnosis (31–33), and preclinically to assess cancer drug resistance (34) and disease progression in multiple sclerosis (35).

To functionally assess alterations in the glutathione biosynthetic pathway, [^{18}F]FSPG was administered intravenously (IV) to 2-3 weeks-old *Asl*$^{Neo/Neo}$ mice and WT littermates, with radiotracer retention dynamically imaged by PET. In all mice, typical healthy tissue [^{18}F]FSPG retention was observed in the salivary glands, thymus, and pancreas, accompanied by renal elimination (Figure 2B). Liver [^{18}F]FSPG retention for *Asl*$^{Neo/Neo}$ mice was 14 ± 4% injected dose (ID)/g, which was 3-fold higher (p=0.002) than that of WT mice (5.2 ± 1.5% ID/g). In PET images of WT mice, [^{18}F]FSPG retention in the liver was just above background, with images dominated by radiotracer retention in the pancreas and kidney. Conversely, it was challenging to distinguish between pancreatic and liver [^{18}F]FSPG retention in *Asl*$^{Neo/Neo}$ mice (Figures 2B, 2C, Figure S4A). We confirmed that the protein expression of xCT in 2-week-old *Asl*$^{Neo/Neo}$ mouse liver was substantially increased compared to WT littermates, which had low baseline expression (Figure 2D). High [^{18}F]FSPG retention was also present in the skin of *Asl*$^{Neo/Neo}$ mice (13 ± 1.8% ID/g) which was not the case in WT littermates (5.3 ± 2.3% ID/g; Figure 2B, 2E; p=0.002; Figure S4B). Increased [^{18}F]FSPG skin retention accompanied gross changes to tissue structure, as shown by hematoxylin and eosin (H&E) staining (Figure 2F). [^{18}F]FSPG is therefore a useful non-invasive marker of aberrant glutathione metabolism in the liver and skin of *Asl*$^{Neo/Neo}$ mice, mediated at least in part through the upregulated expression of the xCT antiporter.

Single intravenous administration of *hASL* mRNA corrects ureagenesis up to 7 days in adult *Asi*$^{Neo/Neo}$ mice

The promising therapeutic effects of mRNA technology have been demonstrated recently in multiple liver inherited metabolic conditions (36, 37). *hASL* mRNA encapsulated in lipid nanoparticles were specifically engineered with *hASL* codon and amino acid sequence optimisation. *hASL* mRNA restored ASL expression (fig. S5A, B) and activity (fig. S5C) in ASL-deficient fibroblasts from patients with ASA compared to a *Luciferase (Luc)* mRNA control lipid nanoparticle. mRNA therapy has transient efficacy and requires re-administration to enable a sustained effect. Thus, we conducted a pharmacokinetic study of *hASL* mRNA in *Asl*$^{Neo/Neo}$ mice to assess the efficacy and duration of effect on the urea cycle. Three-week-old *Asl*$^{Neo/Neo}$ mice received a single IV injection of either *hASL* or *Luc* mRNA at 1 mg mRNA/kg body weight and were sacrificed at 2h, 24h, 72h, or 7 days (Figure 3A). Due to the severity of the phenotype, the experimental design did not include any longitudinal assessment of biomarkers to avoid additional stress that could precipitate the animal's death. Specific cohorts of animals received mRNA therapy at T0 and were harvested at the selected time point. A marked reduction of plasma ammonia (Figure 3B), argininosuccinic acid (Figure 3C), and citrulline (Figure 3D) in dried blood spots as well as urinary orotate (Figure 3E) were observed within 24h of administration in *hASL* mRNA-treated *Asl*$^{Neo/Neo}$ mice compared to the control (*Luc* mRNA)-treated group. This effect was sustained over seven days. The concentrations of these metabolites post-*hASL* mRNA treatment in *Asl*$^{Neo/Neo}$ mice were comparable to the physiological concentrations in WT mice. Plasma ammonia, argininosuccinic acid, and citrulline in dried blood spots were elevated at 2 hours post-injection in the *hASL* mRNA versus *Luc* mRNA

treated group (Figure 3A-C), raising the question of a risk of acute impairment of the urea cycle. No effect on arginine concentrations was observed (Figure S6A). Western blot and immunohistochemistry data in liver showed restored ASL protein abundance at physiological levels at 24h post-administration of *hASL* mRNA (Figures 3F-I, Figure S6B-D). ASL abundance was consistently higher in *hASL*-treated versus the *Luc* mRNA-treated group over this seven-day time course. Liver ASL activity was also restored to physiological levels at 24h and 72h in the *hASL*-treated compared to the *Luc* mRNA-treated group but began to decline by seven days (Figure 3J).

hASL mRNA therapy from birth normalises the phenotype of *Asl*$^{Neo/Neo}$ mice

Pharmacodynamic data showed a single mRNA dose to be efficacious for up to seven days. To better understand the value of this treatment, we initiated a survival study with repeated administration of *hASL* mRNA versus *Luc* mRNA in neonatal *Asl*$^{Neo/Neo}$ pups. Mice received systemic administration of mRNA constructs every seven days with the first IV dose administered at day 1 of life. Due to difficulties injecting young pups, an intraperitoneal (IP) dose of 2 mg/kg at day 8 of life was performed. This twice higher dose was based on liver biodistribution between IV and IP routes, which showed that a two-fold higher IP dose has a similar liver biodistribution as a single IV dose (Figures S7A, 7B). Mice were treated for seven weeks and harvested 48 h after the last injection (Figure 4A). The macroscopic phenotype of *Asl*$^{Neo/Neo}$ mice was restored to that of WT littermates in the *hASL* mRNA treatment group, with normalisation of survival (Figure 4B, p=0.002), growth (Figure 4C, Figure S8A), fur (Figure 4D), and hepatomegaly (Figure S8B). One *hASL* mRNA treated mutant was culled at 24 days of age due to malocclusion, a complication unrelated to the ASL phenotype or mRNA therapy, and was excluded from the analysis. In contrast, *Luc* mRNA-treated *Asl*$^{Neo/Neo}$ littermates showed abnormal fur, impaired growth, and early death within 2 weeks of life (Figure 4B-D).

Animals which survived seven weeks were culled 48 h after the last mRNA injection. Analysis showed normalization of ammonaemia (Figure 4E), argininosuccinic acid (Figure 4F), and citrulline (Figure 4G) concentrations in dried blood spots, and urinary orotate concentrations (Figure 4H) in *hASL* mRNA-treated *Asl*$^{Neo/Neo}$ mice. No significant differences in arginine concentrations in dried blood spots between WT or *Luc* mRNA- or *hASL* mRNA-treated *Asl*$^{Neo/Neo}$ mice were observed (Figure S8C). Elevated plasma amino transferase (ALT) was normalized in the *hASL* mRNA-treated *Asl*$^{Neo/Neo}$ mice (Figure S8D). Longitudinal analysis of plasma ammonia (Figure S8E), argininosuccinic acid, (Figure S8F), and citrulline (Figure S8G) concentrations in dried blood spots, and urinary orotate concentrations (Figure S8H) in *hASL* mRNA-treated *Asl*$^{Neo/Neo}$ mice showed sustained therapeutic benefit over time. Next, functional assessment of urea cycle *in vivo* was measured by quantifying labelled urea in the plasma following the systemic injection of the ^{13}C labelled sodium acetate stable isotope 30 minutes pre-harvest. ^{13}C labelling showed restored ureagenesis in the *hASL* treated *Asl*$^{Neo/Neo}$ mice (Figure 4I). ASL levels in liver assessed by western blot (Figures 4J, 4K) and immunohistochemistry (Figures 4L, 4M) were restored to physiological levels and patterns after *hASL* mRNA therapy. Similar to single-dose short-term therapy, ASL activity in liver was restored to WT physiological levels after *hASL* mRNA therapy in *Asl*$^{Neo/Neo}$ mice at this late time-point

(Figure 4N). Gender analysis showed that there were no sex-related differences in the different efficacy endpoints in the *hASL* mRNA-treated group (Table S3).

hASL mRNA therapy partially rescues the adult phenotype in *Asl*$^{Neo/Neo}$ mice

As untreated *Asl*$^{Neo/Neo}$ mice start dying from 2-3 weeks of age (4), we next wanted to assess whether it was possible to rescue of the severe phenotype of *Asl*$^{Neo/Neo}$ mice after late initiation of *hASL* mRNA therapy. *Asl*$^{Neo/Neo}$ mice received their first IV *hASL* mRNA dose in early adulthood at day 21 of life followed by weekly mRNA administration for up to 8 weeks (Figure 5A). All but one treated mouse survived to the end of the study which died after two injections at day 31 of life. In contrast, *Luc* mRNA-treated mice only survived up to day 37 of life, with most animals dying before day 30 (Figure 5B, p=0.002). *hASL* mRNA-treated *Asl*$^{Neo/Neo}$ mice showed significantly improved growth compared to *Luc* mRNA *Asl*$^{Neo/Neo}$ littermates, however the body weight remained significantly lower than WT littermates (Figure 5C, Figure S9A). The full recovery of hair growth in *hASL* mRNA-treated *Asl*$^{Neo/Neo}$ mice had a similar fur pattern compared to WT (Figure 5D). Liver to body weight ratio remained significantly elevated in both treated *Asl*$^{Neo/Neo}$ mice groups (Figure S9B). Plasma ammonia (Figure 5E), argininosuccinic acid (Figure 5F), and citrulline (Figure 5G) in dried blood spots and urinary orotic acid concentrations (Figure 5H) were reduced after *hASL* mRNA therapy to physiological WT concentrations. In pups treated soon after birth, ^{13}C ureagenesis revealed restored *in vivo* urea cycle function comparable to that of WT in *hASL* mRNA-treated *Asl*$^{Neo/Neo}$ mice (Figure 5I) compared to *Luc* mRNA-treated *Asl*$^{Neo/Neo}$ littermates. There were no significant differences in arginine concentrations between WT, *Luc* mRNA and *hASL* mRNA-treated *Asl*$^{Neo/Neo}$ groups (Figure S9C). ALT concentrations indicated an absence of liver toxicity in the *hASL* mRNA-treated *Asl*$^{Neo/Neo}$ mice compared to WT littermates (Figure S9D). ASL concentrations in the liver, assessed by western blot (Figures 5J, 5K), were restored to physiological concentrations after *hASL* mRNA therapy compared to WT. Liver ASL activity was also significantly improved following *hASL* mRNA compared to *Luc* mRNA in *Asl*$^{Neo/Neo}$ mice (Figure 5L). Gender analysis could not determine any sex differences between the different efficacy endpoints in the *hASL* mRNA-treated group (Figure S10 and Table S4).

[^{18}F]FSPG-PET provides a sensitive pharmacodynamic marker of *hASL* mRNA treatment

To investigate the potential of [^{18}F]FSPG PET as a non-invasive tool of therapeutic efficacy, [^{18}F]FSPG was administered IV to 2 weeks-old untreated and *hASL* mRNA-treated *Asl*$^{Neo/Neo}$ mice (IV administration of 1 mg/kg *hASL* mRNA at birth followed by weekly IP administration of 2 mg/kg mRNA before imaging at 2 weeks of age). Supporting our functional and metabolic data, [^{18}F]FSPG retention was halved in *hASL* mRNA-treated (11 ± 2.0% ID/g) versus untreated *Asl*$^{Neo/Neo}$ mice (22 ± 2.3% ID/g; p = 0.026; Figure 6A, 6B, Figure S11A). At the treatment time-point, however, [^{18}F]FSPG retention was not completely restored to baseline levels seen in WT livers (5.0 ± 2.8% ID/g). In line with lowered [^{18}F]FSPG retention, glutathione metabolism was corrected, with restoration of hepatic liver glutathione in both neonatal and adult treated *Asl*$^{Neo/Neo}$ mice to concentrations similar to those of WT mice (Figure 6C). This restoration of glutathione was associated with a significant reduction of total homocysteine ratio compared to WT in livers from

hASL mRNA-treated versus untreated *Asl*$^{Neo/Neo}$ mice (Figure 6D). In these animals, the expression of cystine/glutamate antiporter system x_c^- was greatly reduced in livers from *hASL* mRNA-treated versus *Asl*$^{Neo/Neo}$ mice (Figure 6E). Conversely, skin [^{18}F]FSPG retention was not affected by mRNA therapy. [^{18}F]FSPG skin retention was 4.2 ± 3.4% ID/g in WT mice, compared to 15 ± 3.7% ID/g and 15 ± 4.2% ID/g in untreated and *hASL* mRNA treated *Asl*$^{Neo/Neo}$ mice, respectively (Figures S11B, S11C).

hASL mRNA therapy corrects the metabolic dysfunction and liver pathophysiology in *Asl*$^{Neo/Neo}$ mice

We wanted to determine the extent of the correction of liver metabolic dysfunction after *hASL* mRNA treatment in *Asl*$^{Neo/Neo}$ mice. To do this, we used RNA-sequencing (RNA-seq) transcriptomic analysis and visualised the overall variation in gene expression across WT and *Asl*$^{Neo/Neo}$ mice treated at birth with either *hASL* or *Luc* mRNA therapy. Principal component analysis showed clustering of the *hASL* mRNA-treated and WT liver samples, suggesting a similar profile of gene expression in both groups. In contrast, *Luc* mRNA treated *Asl*$^{Neo/Neo}$ mice clustered separately (Figure 7A). Next, we analysed differential gene expression identifying all genes with a log2-fold change of >0.1 or < -0.1 and passing an FDR cut off of <0.05. Comparing WT vs *Luc* mRNA *Asl*$^{Neo/Neo}$ groups, we found 2,705 genes to be significantly up- (1,257 genes) or down-regulated (1,448 genes; Figure 7B). Only 7 genes (1 up-regulated and 6 down-regulated) were differentially expressed between WT vs *hASL* mRNA *Asl*$^{Neo/Neo}$ mice livers, thereby demonstrating the efficacy of mRNA therapy in correcting liver dysfunction (Figure 7C). No pathway correlation was observed between these genes, which had different localisation and function (Table S5). This interpretation of the data was supported by the analysis of differential gene expression between mRNA and *hASL* mRNA *Asl*$^{Neo/Neo}$, which similarly to the WT vs *Luc* mRNA *Asl*$^{Neo/Neo}$ comparison, we identified a large number of differentially expressed genes (4,297 genes): 1,962 genes being significantly up-regulated (log2-fold change > 0.1 and FDR < 0.05) and 2,335 being significantly down-regulated (log2-fold change < -0.1 and FDR < 0.05) (Figure 7D).

To further study the dysregulation of glutathione function, the analysis of pathways affecting glutathione metabolism was performed on the RNA-seq data. Our analysis highlighted downregulation of multiple genes involved in glutathione biosynthesis and metabolism alongside alterations of genes of the methionine cycle, transsulfuration, and antioxidant pathways between *Luc* mRNA *Asl*$^{Neo/Neo}$ mice and WT livers (Figure 7E). These findings additionally support disruption of glutathione metabolism in *Asl*$^{Neo/Neo}$ mice, including the downregulation of *Gclc*. These pathways were corrected post-*hASL* mRNA treatment as shown by post-pathway analysis comparison between *hASL* mRNA- and *Luc* mRNA-treated *Asl*$^{Neo/Neo}$ mice (Figure 7E).

NO deficiency is a hallmark of ASA (4, 5). Previous reports have shown that NO donors can upregulate the rate limiting enzyme of glutathione biosynthesis GCL in vascular smooth muscle cells (38) and endothelial cells (39). To test the role of NO on glutathione, we incubated human hepatocellular carcinoma derived Huh7 cells with NO donor S-nitroso-N-acetylpenicillamine (SNAP) versus vehicle (DMSO) control and observed a significant

increase in mRNA expression of both GCL subunits, GCLC (Figure 7F) and GCLM (Figure 7G). This suggests that the normalisation of ASL expression corrects hepatic glutathione metabolism by restoring the NO availability and thereby GCL upregulation (Figure S12).

Discussion

Glutathione is a master antioxidant, a mitochondrial protectant, and regulator of multiple redox processes (40, 41). Glutathione depletion is a well-identified feature of common chronic liver diseases, for example non-alcoholic fatty liver disease, alcoholic liver disease, and cholestasis (42). Generally, raised production of reactive oxygen species causes sustained oxidative stress and scavenges glutathione, although occasionally, compromised glutathione biosynthesis or increased glutathione recycling have been observed (25).

Here we observed glutathione depletion as a key feature of the chronic liver disease in ASA. Glutathione depletion is likely to be multifactorial, with various mechanistic explanations identified in this work, such as decreased biosynthesis, increased degradation, and increased urinary excretion. Although it has been shown that glutathionuria can cause systemic glutathione depletion (43), the normalisation of liver glutathione levels after *hASL* mRNA therapy shows the importance of dysregulated glutathione biosynthesis in the liver. In particular, we observed downregulation of the rate-limiting enzyme of glutathione biosynthesis, GCL, affecting both the catalytic and modifier subunits. The upregulation of the xCT transporter in the liver suggests a feedback mechanism to alleviate the consequences of glutathione depletion. This mechanism has been shown in cancer cells to promote glutathione biosynthesis and thereby cell survival from an increase of the intracellular cysteine pool, and can be observed as well in monogenic liver diseases (21, 44).

These findings contrast with only moderate evidence of oxidative stress and downregulation of genes involved in antioxidant pathways. In ASA livers, the main glutathione-dependent functions and related pathways involved in antioxidant activity and endogenous and xenobiotics detoxification were downregulated. Increased oxidative stress is common in ASA and has been described systemically (5), and in neuronal (9) or endothelial (22) cells. Direct toxicity from argininosuccinate and conjugates (7, 20, 45), and NO deficiency are two pro-oxidant mechanisms. NO deficiency is caused by arginine depletion and subsequent NOS uncoupling (4, 5, 9). NOS uncoupling alters physiological NO synthesis and promotes synthesis of the reactive oxygen species superoxide ion (O_2^-). Additionally, at physiological levels, NO can act as a chain-breaking antioxidant capable of attenuating lipid peroxidation (46). In our study however, the $Asl^{Neo/Neo}$ mouse presents only moderate evidence of hepatic oxidative stress despite evidence of systemic and hepatic NO deficiency.

ASL is the final enzyme required for arginine synthesis in mammals. Arginine is the precursor of NO and consequently, ASA is also a model of inherited NO deficiency. Various clinical symptoms in ASA such as arterial hypertension (5), colitis (47), epilepsy (48), and motor disorder (49) are directly caused by NO deficiency and subsequent downregulation of key physiological processes or metabolic enzymes. NO can upregulate GCL via a non-canonical pathway independent from cGMP in vascular smooth muscle cells (38) and endothelial cells (39). We observed NO-induced *GCL* mRNA upregulation in

Europe PMC Funders Author Manuscripts

human hepatocytes, providing a potential mechanistic link between liver NO deficiency and glutathione depletion, however further studies are required to confirm this link. ASS1 and ASL are both part of the same multiprotein complex jointly with NO synthase. ASL plays a key structural role in maintaining this complex (4). Patients with ASLD have a systemic phenotype, presumably caused partly by systemic NO deficiency (15), which patients with ASSD do not have. Various symptoms affecting the ASLD brain, cardiovascular system, gastrointestinal tract, bone physiology have a pathophysiological explanation based on NO deficiency (9, 22, 47–51). Therefore, the clinical, pathophysiological, and molecular evidences of NO deficiency in ASLD are firmly established, whereas evidence of NO deficiency in ASSD remains limited. The potential extrapolation of ASLD glutathione dysregulation in ASSD remains to be proven.

Glutathione dysregulation and ureagenesis defect are two distinct pathways affected by ASA. Ureagenesis can be assessed with multiple biomarkers such as ammonia, amino acids, orotic acid, and stable isotopes, but this does not inform on the status of glutathione biosynthesis and poorly correlates with chronic liver disease (16). To assess glutathione dysregulation, plasma biomarkers could be assessed, such as homocysteine, cysteine, glutathione, glycine, and glutamate. This study, however, highlights the potential of exploiting defective glutathione biosynthesis with non-invasive [^{18}F]FSPG-PET imaging as a sensitive diagnostic tool to assess the presence of liver disease in ASA. The use of [^{18}F]FSPG-PET imaging is rapidly expanding for clinical cancer imaging (34, 52). Although the use of PET radiotracers in monogenic diseases is a new application, especially in liver indications, we believe this tool will be of interest to academic teams or companies actively developing liver replacement therapies for ASA such as cell or gene (viral (9, 12) or non-viral) therapies. The use of [^{18}F]FSPG-PET imaging in assessing the correction of the chronic liver disease in ASA will not be dependent on the therapeutic approach used: a single systemic AAV-mediated gene therapy injection providing long-term phenotypic correction or repeated intravenous LNP-mRNA administrations with sustained efficacy will both be able to benefit from this imaging modality as a non-invasive marker of clinical improvement. The ability to track the effective correction of impaired glutathione metabolism in the ASA liver provides substantial benefits over other more invasive techniques. Dysregulation of glutathione metabolism and antioxidant pathways were fully corrected following mRNA therapy, as observed in liver transcriptomics and liver glutathione concentrations. Liver [^{18}F]FSPG retention in neonatally-treated animals was halved compared to untreated mice, however radiotracer retention was not completely normalised to WT levels. This could be due to the experimental design, which included a short 2-week period of therapy to achieve age-matched comparison with untreated control *Asl*$^{Neo/Neo}$ animals. We note that the correction was limited to the liver, with no benefit observed in the skin, demonstrating the preferential liver-targeting effect of mRNA therapy as previously described (53).

The lack of effective therapies for both ureagenesis and the chronic liver disease in ASA has promoted the development of various experimental therapies. The autophagy enhancer Tat-Beclin-1 (TB-1) peptide has shown improved ureagenesis along with reduction in hepatocellular injury and glycogen accumulation that may prevent long-term hepatotoxicity (6). Restoration of ureagenesis was achieved using liver-targeting viral-mediated gene

therapies using adenoviral (5, 11), adeno-associated viral (AAV) (9, 12), or lentiviral vectors (10). For viral vector-mediated gene delivery, there are ongoing concerns over capsid immunogenicity and toxicity. There have been recent reports of serious hepatotoxicity following AAV gene delivery in X-linked myotubular myopathy and spinal muscular atrophy (54–57). In parallel, mRNA encapsulated in lipid nanoparticles is emerging as a promising therapy for liver monogenic diseases (58–60). This technology enables the delivery of a functional therapeutic protein to target cells with comparatively longer half-life and lower costs than protein replacement therapies. The absence of acute immunogenicity and integration in the host genome enables safe repeating administration to compensate for mRNA degradation and transient efficacy, becoming a viable alternative to viral vectors (61, 62). Proof of concept mRNA therapy in liver inherited metabolic diseases has increased in frequency in recent years (36, 37, 63, 64), supporting data for early phase clinical trials for ornithine transcarbamylase (NCT04442347), propionic acidemia (NCT04899310), methylmalonic acidemia (NCT04159103), and glycogen storage disease type 1A (NTC05095727). Based on previous proof of concept studies performed in another UCD, arginase deficiency (65, 66), we tested a therapeutic dose of 1 mg/kg of *hASL* mRNA delivered weekly through systemic routes of administration in the $Asl^{Neo/Neo}$ mouse. The treatment of animals from birth showed normalisation of the macroscopic phenotype, plasma metabolites, *in vivo* ureagenesis, and liver ASL expression and activity similar to physiological levels. Comparatively, induction of therapy in early adulthood showed partial but still very effective phenotypic rescue. The observation that arginine concentrations were unable to be rescued, however, remains unexplained. Overall, this study showed proof of concept that mRNA therapy is both safe and efficacious for both early-onset and rescue therapy in a hypomorphic mouse model of ASA with severe phenotype and paves the way for clinical translation. A knock-out mouse model of ASA has previously been described (67) but is no longer available for comparison with our model. Previous translational work in methylmalonic acidaemia has shown similar efficacy of mRNA therapy at same dose and pattern of administration in both severe hypomorphic and knock-out mouse models (63), supporting our findings.

Limitations to our study include the small number of animals per group, which limited the statistical power of some efficacy endpoints. Despite the small sample sizes, however, biochemical and phenotypic differences between WT and $Asl^{Neo/Neo}$ mice were extensive, as was the rescue effect of mRNA treatment. Small group sizes, however, limited our ability to assess the sex differences of thiol metabolites in patients with urea cycle defects and mRNA-treated $Asl^{Neo/Neo}$ mice. Additionally, mRNA therapy was studied up to 7 and 9 weeks in neonatally- and adult-treated $Asl^{Neo/Neo}$ mice, respectively. We cannot exclude that an extended duration of mRNA therapy in ASA might have revealed only partial sustained efficacy due to single organ (liver) correction in this systemic disease. Due to the study design, long-term LNP-related toxicity, a critical aspect for clinical translation, was not studied, although this type of toxicity has not been shown in other LNP-mRNA studies in other murine models of liver inherited metabolic diseases (36, 37).

In conclusion, our study shows dysfunction of glutathione metabolism in both ASL-deficient patients and an $Asl^{Neo/Neo}$ mouse model, whilst mRNA-LNP therapy corrected both glutathione metabolism and ureagenesis *in vivo*. Preliminary data suggests that glutathione

biosynthesis in the liver is regulated by NO availability. Furthermore, we demonstrated the potential of [^{18}F]FSPG-PET as a companion diagnostic to assess liver disease and therapeutic efficacy in ASA. These insights into the liver pathophysiology of ASA provide perspectives for targeted therapies, which could change the outcome of patients affected by this rare disease with currently high unmet needs and limited therapeutic options.

Materials and Methods

Study design

This study was designed to investigate hepatic glutathione metabolism and its role in the chronic liver disease in ASA. To assess glutathione metabolism in ASA, we first measured thiol metabolites in plasma of ASL-deficient patients. To investigate the cause of dysregulated glutathione metabolism in ASA, we measured plasma and liver thiol metabolites in *Asl*$^{Neo/Neo}$ mouse model and performed liver untargeted proteomics. Next, we monitored redox changes in ASL-deficient murine liver using [^{18}F]FSPG-PET. We then investigated the therapeutic potential of *hASL* mRNA in correcting dysregulated glutathione metabolism. We first assessed *hASL* mRNA efficacy by ASL supraphysiological overexpression and correction in human derived liver cell line and ASL-deficient fibroblasts, respectively. To evaluate this, we designed pharmacokinetic studies after systemic administration in *Asl*$^{Neo/Neo}$ animals of *hASL* mRNA or *Luc* mRNA. Untreated WT littermates were used as controls. *Asl*$^{Neo/Neo}$ mice were administered IV at 3-weeks of age and harvested at different timepoints, 2, 24, 72 h or 7 days. We then designed two survival studies for *Asl*$^{Neo/Neo}$ animals treated from birth and early adulthood. We initially assessed whether ureagenesis, the main cause of mortality in these *Asl*$^{Neo/Neo}$ mice, was corrected. In the first study, neonatal pups at day 1 were administered mRNA systemically weekly up to 7-weeks of age. In the second survival study of animals treated from early adulthood, mice were given weekly IV administration from day 21 onwards up to 9-weeks of age. Efficacy endpoints were survival, growth, fur pattern, plasma ammonia and urea-cycle related amino acids measured in dried blood spot, urine orotic acid, ^{13}C ureagenesis, liver western blot, immunostaining and enzyme activity for ASL. All harvests were performed 48 h after the last injection. Mutant mice were assigned randomly to study groups. All animals were monitored and weighted daily. After assessment of the therapeutic effect on ureagenesis, we assessed the therapeutic effect of *hASL* mRNA on dysregulated glutathione metabolism using [^{18}F]FSPG-PET and thiol metabolites. Analysis was performed blindly to genotype. We assessed liver transcriptomics in control and treated *Asl*$^{Neo/Neo}$ mice. We investigated the expression of glutathione synthetic enzymes in vitro in the presence of NO donor. *n=3* independent experiments were conducted for each *in vitro* experiment of the study. Animal procedures were approved by institutional ethical review and performed per UK home office licenses PP9223137, 70/14300 and PEFC6ABF1.

Statistical analysis

Data was analysed and represented using Graphpad Prism 9.0 software. Figures shown mean +/- standard deviation. Kaplan-Meier survival curves were analysed using log-rank test. Pairwise comparison of means was performed using Student's *t* test (two-sided) for comparison of two groups, assuming that the data was normally distributed. Simple linear

Europe PMC Funders Author Manuscripts

regression analysis comparing average slopes per group was performed to compare growth curves. Due to early death of *Luc*-mRNA treated $Asl^{Neo/Neo}$ mice, the analysis comparing this cohort was performed for the duration of the survival of these animals. For treated adult animals, analysis was performed using data from the timepoint of the first injection of LNP-mRNA. One-way ANOVA with Tukey's post-hoc test comparison or two-way ANOVA with Šídák's post-hoc test comparison was used to compare more than 2 groups. Log transformation was used to compare groups lacking normal distribution. All statistical results for figures 1-7 are summarised in table S6A-G.

Supplementary Material

Refer to Web version on PubMed Central for supplementary material.

Acknowledgements

The authors would like to thank Eman Khalil for assistance with xCT western blotting, Phil Blower, Kavitha Sunassee, Jana Kim, Floyd Laniyan, Samantha Richards, Rebecca Towns, Katherine Howett, Mirabela Bandol and the staff from Biological services for help with PPL licence, breeding and maintenance of the ASL colony at King's College London and University College London. We are grateful to the patients, families and metabolic physicians (Dr Spyros Batzios, Dr Clare Beesley, Dr Alexander Broomfield, Dr Anupam Chakrapani, Dr Maureen Cleary, Dr Dr James Davison, Emma Footitt, Dr Stephanie Grunewald, Dr Karin Tuschl, Dr Mildrid Yeo) from Great Ormond Street Hospital for Children in London, UK for anonymously sharing data for this study. Some graphical illustrations were created with Biorender.com.

Funding

This work was supported by funding from Moderna Inc. (JB), the United Kingdom Medical Research Council Clinician Scientist Fellowship MR/T008024/1 (JB), London Advanced Therapy Confidence in Collaboration in Advanced Therapies award (2CiC017) (JB, THW), a Wellcome Trust Senior Fellowship 220221/Z/20/Z (THW), the CRUK City of London Centre Award C7893/A26233 (THW), and the NIHR Great Ormond Street Hospital Biomedical Research Centre (JB, PG, PBM, SE). The views expressed are those of the author(s) and not necessarily those of the NHS, the NIHR or the Department of Health. This research was funded in whole or in part by Wellcome Trust Senior Fellowship 220221/Z/20/Z, a cOAlition S organization. The author will make the Author Accepted Manuscript (AAM) version available under a CC BY copyright license.

Data and materials availability

All data associated with this study are present in the paper or the Supplementary Materials. Requests for ASL LNP-mRNA should be made directly to Moderna Inc. under a material transfer agreement. Requests for data should be addressed to JB or THW. The transcriptomic dataset is available on NCBI Gene Expression Omnibus, accession number GSE222874.

References

1. Summar ML, Koelker S, Freedenberg D, Le Mons C, Haberle J, Lee HS, Kirmse B. The incidence of urea cycle disorders. Mol Genet Metab. 2013; 110: 179–180. [PubMed: 23972786]
2. Baruteau J, Diez-Fernandez C, Lerner S, Ranucci G, Gissen P, Dionisi-Vici C, Nagamani S, Erez A, Häberle J. Argininosuccinic aciduria: Recent pathophysiological insights and therapeutic prospects. J Inherit Metab Dis. 2019; 42: 1147–1161. [PubMed: 30723942]
3. Erez A. Argininosuccinic aciduria: from a monogenic to a complex disorder. Genet Med. 2013; 15: 251–257. [PubMed: 23306800]
4. Erez A, Nagamani SC, Shchelochkov OA, Premkumar MH, Campeau PM, Chen Y, Garg HK, Li L, Mian A, Bertin TK, Black JO, et al. Requirement of argininosuccinate lyase for systemic nitric oxide production. Nat Med. 2011; 17: 1619–1626. [PubMed: 22081021]

5. Nagamani SC, Campeau PM, Shchelochkov OA, Premkumar MH, Guse K, Brunetti-Pierri N, Chen Y, Sun Q, Tang Y, Palmer D, Reddy AK, et al. Nitric-oxide supplementation for treatment of long-term complications in argininosuccinic aciduria. Am J Hum Genet. 2012; 90: 836–846. [PubMed: 22541557]
6. Soria LR, Gurung S, De Sabbata G, Perocheau DP, De Angelis A, Bruno G, Polishchuk E, Paris D, Cuomo P, Motta A, Orford M, et al. Beclin-1-mediated activation of autophagy improves proximal and distal urea cycle disorders. EMBO Mol Med. 2021; 13 e13158 [PubMed: 33369168]
7. Seminotti B, da Silva JC, Ribeiro RT, Leipnitz G, Wajner M. Free Radical Scavengers Prevent Argininosuccinic Acid-Induced Oxidative Stress in the Brain of Developing Rats: a New Adjuvant Therapy for Argininosuccinate Lyase Deficiency? Mol Neurobiol. 2020; 57: 1233–1244. [PubMed: 31707633]
8. Nagamani SC, Erez A, Lee B. Argininosuccinate lyase deficiency. Genet Med. 2012; 14: 501–507. [PubMed: 22241104]
9. Baruteau J, Perocheau DP, Hanley J, Lorvellec M, Rocha-Ferreira E, Karda R, Ng J, Suff N, Diaz JA, Rahim AA, Hughes MP, et al. Argininosuccinic aciduria fosters neuronal nitrosative stress reversed by Asl gene transfer. Nat Commun. 2018; 9 3505 [PubMed: 30158522]
10. Touramanidou, L; Perocheau, D; Gurung, S; Cozmescu, AC; Waddington, SN; Counsell, JR; Gissen, P; Baruteau, J. European Society of Gene and Cell Therapy (ESGCT); Virtual Congress; 2021.
11. Burrage LC, Madan S, Li X, Ali S, Mohammad M, Stroup BM, Jiang MM, Cela R, Bertin T, Jin Z, Dai J, et al. Chronic liver disease and impaired hepatic glycogen metabolism in argininosuccinate lyase deficiency. JCI Insight. 2020; 5
12. Ashley SN, Nordin JML, Buza EL, Greig JA, Wilson JM. Adeno-associated viral gene therapy corrects a mouse model of argininosuccinic aciduria. Mol Genet Metab. 2018; 125: 241–250. [PubMed: 30253962]
13. Ranucci G, Rigoldi M, Cotugno G, Bernabei SM, Liguori A, Gasperini S, Goffredo BM, Martinelli D, Monti L, Francalanci P, Candusso M, et al. Chronic liver involvement in urea cycle disorders. J Inherit Metab Dis. 2019; 42: 1118–1127. [PubMed: 31260111]
14. Bigot A, Tchan MC, Thoreau B, Blasco H, Maillot F. Liver involvement in urea cycle disorders: a review of the literature. Journal of inherited metabolic disease. 2017; 40: 757–769. [PubMed: 28900784]
15. Baruteau J, Jameson E, Morris AA, Chakrapani A, Santra S, Vijay S, Kocadag H, Beesley CE, Grunewald S, Murphy E, Cleary M, et al. Expanding the phenotype in argininosuccinic aciduria: need for new therapies. J Inherit Metab Dis. 2017; 40: 357–368. [PubMed: 28251416]
16. Nagamani SCS, Ali S, Izem R, Schady D, Masand P, Shneider BL, Leung DH, Burrage LC. Biomarkers for liver disease in urea cycle disorders. Mol Genet Metab. 2021; 133: 148–156. [PubMed: 33846069]
17. Tuchman M, Lee B, Lichter-Konecki U, Summar ML, Yudkoff M, Cederbaum SD, Kerr DS, Diaz GA, Seashore MR, Lee HS, McCarter RJ, et al. Cross-sectional multicenter study of patients with urea cycle disorders in the United States. Mol Genet Metab. 2008; 94: 397–402. [PubMed: 18562231]
18. Marble M, McGoey RR, Mannick E, Keats B, Ng SS, Deputy S, Gereighty H, Schmidt-Sommerfeld E. Living related liver transplant in a patient with argininosuccinic aciduria and cirrhosis: metabolic follow-up. J Pediatr Gastroenterol Nutr. 2008; 46: 453–456. [PubMed: 18367960]
19. Zimmermann A, Bachmann C, Baumgartner R. Severe liver fibrosis in argininosuccinic aciduria. Arch Pathol Lab Med. 1986; 110: 136–140. [PubMed: 3753845]
20. Nagamani SC, Shchelochkov OA, Mullins MA, Carter S, Lanpher BC, Sun Q, Kleppe S, Erez A, O'Brian Smith E, Marini JC, Lee B. A randomized controlled trial to evaluate the effects of high-dose versus low-dose of arginine therapy on hepatic function tests in argininosuccinic aciduria. Mol Genet Metab. 2012; 107: 315–321. [PubMed: 23040521]
21. Liu J, Xia X, Huang P. xCT: A Critical Molecule That Links Cancer Metabolism to Redox Signaling. Mol Ther. 2020; 28: 2358–2366. [PubMed: 32931751]

22. Kho J, Tian X, Wong WT, Bertin T, Jiang MM, Chen S, Jin Z, Shchelochkov OA, Burrage LC, Reddy AK, Jiang H, et al. Argininosuccinate Lyase Deficiency Causes an Endothelial-Dependent Form of Hypertension. Am J Hum Genet. 2018; 103: 276–287. [PubMed: 30075114]

23. Cortese-Krott MM, Koning A, Kuhnle GGC, Nagy P, Bianco CL, Pasch A, Wink DA, Fukuto JM, Jackson AA, van Goor H, Olson KR, et al. The Reactive Species Interactome: Evolutionary Emergence, Biological Significance, and Opportunities for Redox Metabolomics and Personalized Medicine. Antioxid Redox Signal. 2017; 27: 684–712. [PubMed: 28398072]

24. Jiang X, Zhou Q, Du B, Li S, Huang Y, Chi Z, Lee WM, Yu M, Zheng J. Noninvasive monitoring of hepatic glutathione depletion through fluorescence imaging and blood testing. Sci Adv. 2021; 7

25. Lu SC. Regulation of glutathione synthesis. Mol Aspects Med. 2009; 30: 42–59. [PubMed: 18601945]

26. Baruteau J, Diez-Fernandez C, Lerner S, Ranucci G, Gissen P, Dionisi-Vici C, Nagamani S, Erez A, Haberle J. Argininosuccinic aciduria: Recent pathophysiological insights and therapeutic prospects. J Inherit Metab Dis. 2019; 42: 1147–1162. [PubMed: 30723942]

27. Kolker S, Valayannopoulos V, Burlina AB, Sykut-Cegielska J, Wijburg FA, Teles EL, Zeman J, Dionisi-Vici C, Baric I, Karall D, Arnoux JB, et al. The phenotypic spectrum of organic acidurias and urea cycle disorders. Part 2: the evolving clinical phenotype. J Inherit Metab Dis. 2015; 38: 1059–1074. [PubMed: 25875216]

28. Abdulle AE, van Roon AM, Smit AJ, Pasch A, van Meurs M, Bootsma H, Bakker SJL, Said MY, Fernandez BO, Feelisch M, van Goor H, et al. Rapid free thiol rebound is a physiological response following cold-induced vasoconstriction in healthy humans, primary Raynaud and systemic sclerosis. Physiol Rep. 2019; 7 e14017 [PubMed: 30916482]

29. Owen JB, Butterfield DA. Measurement of oxidized/reduced glutathione ratio. Methods Mol Biol. 2010; 648: 269–277. [PubMed: 20700719]

30. Koppula P, Zhang Y, Zhuang L, Gan B. Amino acid transporter SLC7A11/xCT at the crossroads of regulating redox homeostasis and nutrient dependency of cancer. Cancer Commun (Lond). 2018; 38: 12. [PubMed: 29764521]

31. McCormick PN, Greenwood HE, Glaser M, Maddocks ODK, Gendron T, Sander K, Gowrishankar G, Hoehne A, Zhang T, Shuhendler AJ, Lewis DY, et al. Assessment of Tumor Redox Status through (S)-4-(3-[(18)F]fluoropropyl)-L-Glutamic Acid PET Imaging of System xc (-) Activity. Cancer Res. 2019; 79: 853–863. [PubMed: 30401715]

32. Greenwood HE, McCormick PN, Gendron T, Glaser M, Pereira R, Maddocks ODK, Sander K, Zhang T, Koglin N, Lythgoe MF, Arstad E, et al. Measurement of Tumor Antioxidant Capacity and Prediction of Chemotherapy Resistance in Preclinical Models of Ovarian Cancer by Positron Emission Tomography. Clin Cancer Res. 2019; 25: 2471–2482. [PubMed: 30651275]

33. Greenwood HE, Edwards R, Koglin N, Berndt M, Baark F, Kim J, Firth G, Khalil E, Mueller A, Witney TH. Radiotracer stereochemistry affects substrate affinity and kinetics for improved imaging of system xC (-) in tumors. Theranostics. 2022; 12: 1921–1936. [PubMed: 35198080]

34. Baek S, Choi CM, Ahn SH, Lee JW, Gong G, Ryu JS, Oh SJ, Bacher-Stier C, Fels L, Koglin N, Hultsch C, et al. Exploratory clinical trial of (4S)-4-(3-[18F]fluoropropyl)-L-glutamate for imaging xC-transporter using positron emission tomography in patients with non-small cell lung or breast cancer. Clin Cancer Res. 2012; 18: 5427–5437. [PubMed: 22893629]

35. Hoehne A, James ML, Alam IS, Ronald JA, Schneider B, D'Souza A, Witney TH, Andrews LE, Cropper HC, Behera D, Gowrishankar G, et al. [(18)F]FSPG-PET reveals increased cystine/glutamate antiporter (xc-) activity in a mouse model of multiple sclerosis. J Neuroinflammation. 2018; 15: 55. [PubMed: 29471880]

36. An D, Schneller JL, Frassetto A, Liang S, Zhu X, Park JS, Theisen M, Hong SJ, Zhou J, Rajendran R, Levy B, et al. Systemic Messenger RNA Therapy as a Treatment for Methylmalonic Acidemia. Cell Rep. 2017; 21: 3548–3558. [PubMed: 29262333]

37. Jiang L, Park JS, Yin L, Laureano R, Jacquinet E, Yang J, Liang S, Frassetto A, Zhuo J, Yan X, Zhu X, et al. Dual mRNA therapy restores metabolic function in long-term studies in mice with propionic acidemia. Nat Commun. 2020; 11 5339 [PubMed: 33087718]

38. Moellering D, McAndrew J, Patel RP, Cornwell T, Lincoln T, Cao X, Messina JL, Forman HJ, Jo H, Darley-Usmar VM. Nitric oxide-dependent induction of glutathione synthesis through

Europe PMC Funders Author Manuscripts

increased expression of gamma-glutamylcysteine synthetase. Arch Biochem Biophys. 1998; 358: 74–82. [PubMed: 9750167]

39. Moellering D, Mc Andrew J, Patel RP, Forman HJ, Mulcahy RT, Jo H, Darley-Usmar VM. The induction of GSH synthesis by nanomolar concentrations of NO in endothelial cells: a role for gamma-glutamylcysteine synthetase and gamma-glutamyl transpeptidase. FEBS Lett. 1999; 448: 292–296. [PubMed: 10218495]
40. Feelisch M, Cortese-Krott MM, Santolini J, Wootton SA, Jackson AA. Systems redox biology in health and disease. EXCLI J. 2022; 21: 623–646. [PubMed: 35721574]
41. Meister A. Glutathione metabolism. Methods Enzymol. 1995; 251: 3–7. [PubMed: 7651209]
42. Vairetti M, Di Pasqua LG, Cagna M, Richelmi P, Ferrigno A, Berardo C. Changes in Glutathione Content in Liver Diseases: An Update. Antioxidants (Basel). 2021; 10
43. Lieberman MW, Wiseman AL, Shi ZZ, Carter BZ, Barrios R, Ou CN, Chevez-Barrios P, Wang Y, Habib GM, Goodman JC, Huang SL, et al. Growth retardation and cysteine deficiency in gamma-glutamyl transpeptidase-deficient mice. Proc Natl Acad Sci U S A. 1996; 93: 7923–7926. [PubMed: 8755578]
44. Liu X, Zhang Y, Zhuang L, Olszewski K, Gan B. NADPH debt drives redox bankruptcy: SLC7A11/xCT-mediated cystine uptake as a double-edged sword in cellular redox regulation. Genes Dis. 2021; 8: 731–745. [PubMed: 34522704]
45. Aoyagi K, Nagase S, Gotoh M, Akiyama K, Satoh M, Hirayama A, Koyama A. Role of reactive oxygen and argininosuccinate in guanidinosuccinate synthesis in isolated rat hepatocytes. Enzyme Protein. 1996; 49: 205–211. [PubMed: 9030887]
46. Wink DA, Miranda KM, Espey MG, Pluta RM, Hewett SJ, Colton C, Vitek M, Feelisch M, Grisham MB. Mechanisms of the antioxidant effects of nitric oxide. Antioxid Redox Signal. 2001; 3: 203–213. [PubMed: 11396476]
47. Stettner N, Rosen C, Bernshtein B, Gur-Cohen S, Frug J, Silberman A, Sarver A, Carmel-Neiderman NN, Eilam R, Biton I, Pevsner-Fischer M, et al. Induction of Nitric-Oxide Metabolism in Enterocytes Alleviates Colitis and Inflammation-Associated Colon Cancer. Cell Rep. 2018; 23: 1962–1976. [PubMed: 29768197]
48. Lerner S, Anderzhanova E, Verbitsky S, Eilam R, Kuperman Y, Tsoory M, Kuznetsov Y, Brandis A, Mehlman T, Mazkereth R, U. Neuropsychologists. et al. ASL Metabolically Regulates Tyrosine Hydroxylase in the Nucleus Locus Coeruleus. Cell Rep. 2019; 29: 2144–2153. e2147 [PubMed: 31747589]
49. Lerner S, Eilam R, Adler L, Baruteau J, Kreiser T, Tsoory M, Brandis A, Mehlman T, Ryten M, Botia JA, Ruiz SG, et al. ASL expression in ALDH1A1(+) neurons in the substantia nigra metabolically contributes to neurodegenerative phenotype. Hum Genet. 2021; 140: 1471–1485. [PubMed: 34417872]
50. Premkumar MH, Sule G, Nagamani SC, Chakkalakal S, Nordin A, Jain M, Ruan MZ, Bertin T, Dawson B, Zhang J, Schady D, et al. Argininosuccinate lyase in enterocytes protects from development of necrotizing enterocolitis. Am J Physiol Gastrointest Liver Physiol. 2014; 307: G347–354. [PubMed: 24904080]
51. Jin Z, Kho J, Dawson B, Jiang MM, Chen Y, Ali S, Burrage LC, Grover M, Palmer DJ, Turner DL, Ng P, et al. Nitric oxide modulates bone anabolism through regulation of osteoblast glycolysis and differentiation. J Clin Invest. 2021; 131
52. Kavanaugh G, Williams J, Morris AS, Nickels ML, Walker R, Koglin N, Stephens AW, Washington MK, Geevarghese SK, Liu Q, Ayers D, et al. Utility of [(18)F]FSPG PET to Image Hepatocellular Carcinoma: First Clinical Evaluation in a US Population. Mol Imaging Biol. 2016; 18: 924–934. [PubMed: 27677886]
53. Jiang L, Berraondo P, Jerico D, Guey LT, Sampedro A, Frassetto A, Benenato KE, Burke K, Santamaria E, Alegre M, Pejenaute A, et al. Systemic messenger RNA as an etiological treatment for acute intermittent porphyria. Nat Med. 2018; 24: 1899–1909. [PubMed: 30297912]
54. Baruteau J, Waddington SN, Alexander IE, Gissen P. Gene therapy for monogenic liver diseases: clinical successes, current challenges and future prospects. J Inherit Metab Dis. 2017; 40: 497–517. [PubMed: 28567541]

55. Wilson JM, Flotte TR. Moving Forward After Two Deaths in a Gene Therapy Trial of Myotubular Myopathy. Human gene therapy. 2020; 31: 695–696. [PubMed: 32605399]
56. Philippidis A. Fourth Boy Dies in Clinical Trial of Astellas' AT132. Hum Gene Ther. 2021; 32: 1008–1010. [PubMed: 34662231]
57. Guillou J, de Pellegars A, Porcheret F, Fremeaux-Bacchi V, Allain-Launay E, Debord C, Denis M, Pereon Y, Barnerias C, Desguerre I, Roussey G, et al. Fatal thrombotic microangiopathy case following adeno-associated viral SMN gene therapy. Blood Adv. 2022; 6: 4266–4270. [PubMed: 35584395]
58. Sahin U, Karikó K, Türeci Ö. mRNA-based therapeutics--developing a new class of drugs. Nat Rev Drug Discov. 2014; 13: 759–780. [PubMed: 25233993]
59. Berraondo P, Martini PGV, Avila MA, Fontanellas A. Messenger RNA therapy for rare genetic metabolic diseases. Gut. 2019; 68: 1323–1330. [PubMed: 30796097]
60. Córdoba KM, Jericó D, Sampedro A, Jiang L, Iraburu MJ, Martini PGV, Berraondo P, Avila MA, Fontanellas A. Messenger RNA as a personalized therapy: The moment of truth for rare metabolic diseases. Int Rev Cell Mol Biol. 2022; 372: 55–96. [PubMed: 36064267]
61. Hou X, Zaks T, Langer R, Dong Y. Lipid nanoparticles for mRNA delivery. Nat Rev Mater. 2021; 6: 1078–1094. [PubMed: 34394960]
62. Damase TR, Sukhovershin R, Boada C, Taraballi F, Pettigrew RI, Cooke JP. The Limitless Future of RNA Therapeutics. Front Bioeng Biotechnol. 2021; 9 628137 [PubMed: 33816449]
63. An D, Frassetto A, Jacquinet E, Eybye M, Milano J, DeAntonis C, Nguyen V, Laureano R, Milton J, Sabnis S, Lukacs CM, et al. Long-term efficacy and safety of mRNA therapy in two murine models of methylmalonic acidemia. EBioMedicine. 2019; 45: 519–528. [PubMed: 31303505]
64. Yu H, Brewer E, Shields M, Crowder M, Sacchetti C, Soontornniyomkij B, Dou D, Clemente B, Sablad M, Chivukula P, Hughes S, et al. Restoring ornithine transcarbamylase (OTC) activity in an OTC-deficient mouse model using LUNAR-OTC mRNA. Clinical and Translational Discovery. 2022; 2: e33.
65. Khoja S, Liu XB, Truong B, Nitzahn M, Lambert J, Eliav A, Nasser E, Randolph E, Burke KE, White R, Zhu X, et al. Intermittent lipid nanoparticle mRNA administration prevents cortical dysmyelination associated with arginase deficiency. Mol Ther Nucleic Acids. 2022; 28: 859–874. [PubMed: 35694211]
66. Truong B, Allegri G, Liu XB, Burke KE, Zhu X, Cederbaum SD, Häberle J, Martini PGV, Lipshutz GS. Lipid nanoparticle-targeted mRNA therapy as a treatment for the inherited metabolic liver disorder arginase deficiency. Proc Natl Acad Sci U S A. 2019; 116: 21150–21159. [PubMed: 31501335]
67. Reid Sutton V, Pan Y, Davis EC, Craigen WJ. A mouse model of argininosuccinic aciduria: biochemical characterization. Mol Genet Metab. 2003; 78: 11–16. [PubMed: 12559843]
68. Nelson J, Sorensen EW, Mintri S, Rabideau AE, Zheng W, Besin G, Khatwani N, Su SV, Miracco EJ, Issa WJ, Hoge S, et al. Impact of mRNA chemistry and manufacturing process on innate immune activation. Sci Adv. 2020; 6 eaaz6893 [PubMed: 32637598]
69. Edwards R, Greenwood HE, McRobbie G, Khan I, Witney TH. Robust and Facile Automated Radiosynthesis of [(18)F]FSPG on the GE FASTlab. Mol Imaging Biol. 2021; 23: 854–864. [PubMed: 34013395]
70. Greenwood HE, Nyitrai Z, Mocsai G, Hobor S, Witney TH. High-Throughput PET/CT Imaging Using a Multiple-Mouse Imaging System. J Nucl Med. 2020; 61: 292–297. [PubMed: 31519806]
71. Prinsen H, Schiebergen-Bronkhorst BGM, Roeleveld MW, Jans JJM, de Sain-van der Velden MGM, Visser G, van Hasselt PM, Verhoeven-Duif NM. Rapid quantification of underivatized amino acids in plasma by hydrophilic interaction liquid chromatography (HILIC) coupled with tandem mass-spectrometry. J Inherit Metab Dis. 2016; 39: 651–660. [PubMed: 27099181]
72. Janero DR, Bryan NS, Saijo F, Dhawan V, Schwalb DJ, Warren MC, Feelisch M. Differential nitros(yl)ation of blood and tissue constituents during glyceryl trinitrate biotransformation in vivo. Pro Natl Acad Sci U S A. 2004; 101: 16958–16963.
73. McKenna HT, O'Brien KA, Fernandez BO, Minnion M, Tod A, McNally BD, West JA, Griffin JL, Grocott MP, Mythen MG, Feelisch M, et al. Divergent trajectories of cellular bioenergetics,

intermediary metabolism and systemic redox status in survivors and non-survivors of critical illness. Redox Biol. 2021; 41 101907 [PubMed: 33667994]

74. Sutton TR, Minnion M, Barbarino F, Koster G, Fernandez BO, Cumpstey AF, Wischmann P, Madhani M, Frenneaux MP, Postle AD, Cortese-Krott MM, et al. A robust and versatile mass spectrometry platform for comprehensive assessment of the thiol redox metabolome. Redox Biol. 2018; 16: 359–380. [PubMed: 29627744]
75. Kok CY, Cunningham SC, Carpenter KH, Dane AP, Siew SM, Logan GJ, Kuchel PW, Alexander IE. Adeno-associated virus-mediated rescue of neonatal lethality in argininosuccinate synthetase-deficient mice. Mol Ther. 2013; 21: 1823–1831. [PubMed: 23817206]
76. Love MI, Huber W, Anders S. Moderated estimation of fold change and dispersion for RNA-seq data with DESeq2. Genome Biol. 2014; 15: 550. [PubMed: 25516281]
77. Wickham, H. ggplot2: Elegant Graphics for Data Analysis. Springer-Verlag; New York: 2016. ISBN 978-3-319-24277-4https://ggplot2.tidyverse.org
78. Bliss E, Heywood WE, Benatti M, Sebire NJ, Mills K. An optimised method for the proteomic profiling of full thickness human skin. Biol Proced Online. 2016; 18: 15. [PubMed: 27445641]

Europe PMC Funders Author Manuscripts

Europe PMC Funders Author Manuscripts

One-sentence summary

Argininosuccinic aciduria causes defective glutathione metabolism, which can be monitored by PET and corrected by liver-targeted mRNA therapy in mice.

Europe PMC Funders Author Manuscripts

Editor's summary

Genetic argininosuccinate lyase (ASL) deficiency results in excess blood ammonia and downstream neurological and metabolic impairments. Gurung *et al.* report that ASL deficiency in patients also causes dysregulation of glutathione synthesis. Lipid nanoparticle-encapsulated human *ASL* mRNA corrected glutathione and urea metabolism and ameliorated liver disease symptoms in a mouse model of the disease. PET imaging of the mice using further suggested that [^{18}F]FSPG, as a readout of glutathione synthesis, may have utility in monitoring the extent of disease and treatment response. – Catherine Charneski

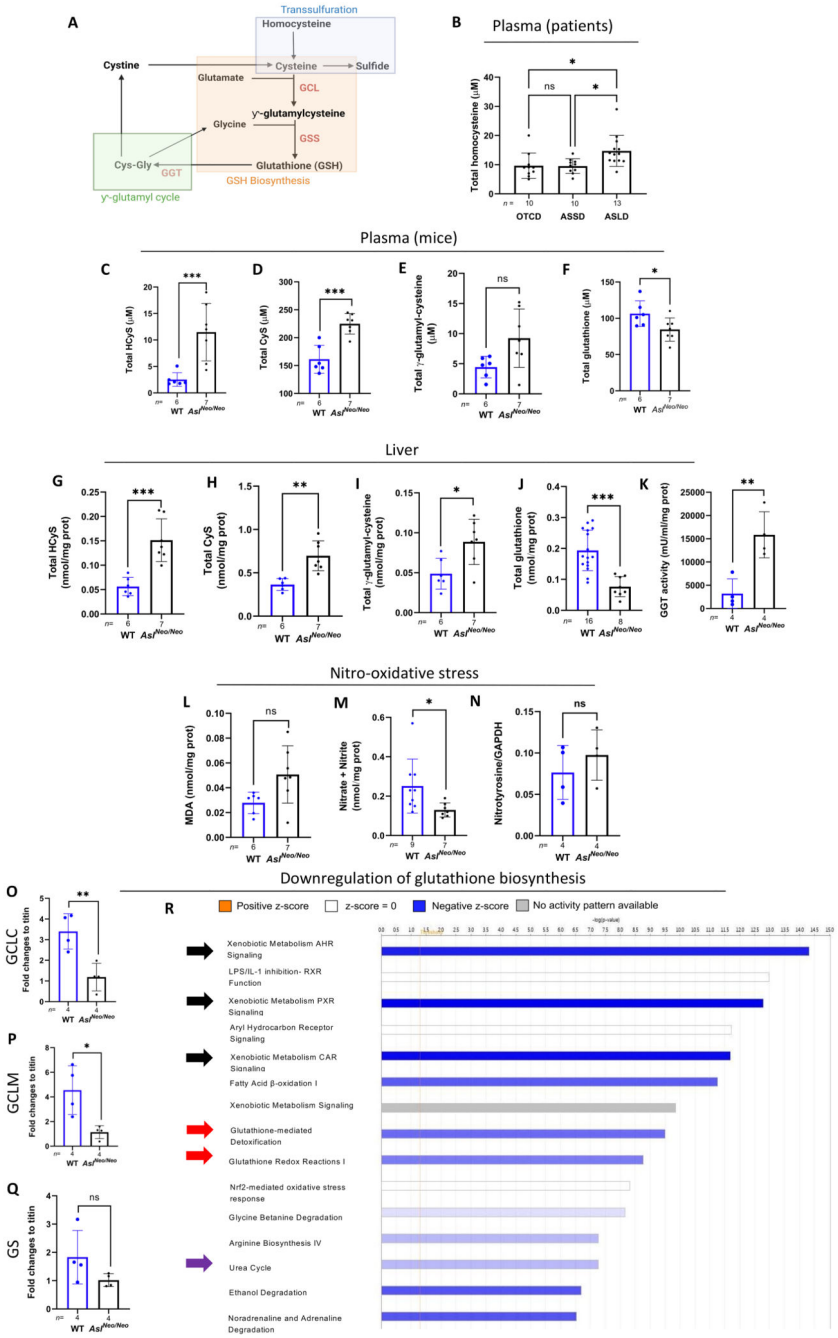

Figure 1. ASL-deficient patients and *Asl*$^{Neo/Neo}$ mice show dysfunction of glutathione metabolism despite limited evidence of oxidative stress.

(**A**) Glutathione biosynthesis requires precursor metabolites glutamate, glycine, and cysteine, the latter being an intermediary metabolite from the transsulfuration pathway. Glutathione is degraded into cysteine-glycine by γ-glutamyl transferase through the γ-glutamyl cycle. (**B**) Mean of plasma total homocysteine in patients with OTCD (n=11-13), ASSD (n=10), ASLD (n=13). Plasma (**C**) total homocysteine, (**D**) cysteine, (**E**) γ-glutamyl-cysteine, (**F**) total glutathione, and liver (**G**) homocysteine, (**H**) cysteine, (**I**) γ-glutamyl-

Europe PMC Funders Author Manuscripts

cysteine total thiols, and (**J**) total glutathione in 2-week old *Asl*$^{Neo/Neo}$ mice and WT littermates. (**K**) Hepatic GGT activity measured in 2-week-old *Asl*$^{Neo/Neo}$ mice and WT littermates. (**L**) Lipid peroxidation measured by thiobarbituric acid reactive substances in *Asl*$^{Neo/Neo}$ mice and WT littermates. (**M**) Nitric oxide metabolites (nitrite and nitrate) in liver samples of *Asl*$^{Neo/Neo}$ mice and WT littermates. (**N**) Quantification of liver nitrotyrosine by western blot between *Asl*$^{Neo/Neo}$ mice and WT. mRNA expression of GCL subunits (**O**) GCLC, (**P**) GCLM, and (**Q**) GS in liver of *Asl*$^{Neo/Neo}$ mice compared to WT littermates. Urea cycle dysfunction is shown by purple arrows. (**R**) Ingenuity pathway analysis of liver untargeted proteomics in *Asl*$^{Neo/Neo}$ mice compared to WT littermates, highlighting downregulation of the main glutathione functions, detoxification of xenobiotic and endogenous compounds (black arrows), antioxidant activity (red arrows). (B) One-way ANOVA with Tukey's post-hoc test. (C) Unpaired two-tailed Student's *t* test performed on log-transformed data. Graph displays not transformed data. (D-Q) Unpaired two-tailed Student's *t* test; * $p<0.05$, ** $p<0.01$, *** $p<0.001$, ns not significant. ASSD: argininosuccinate synthase deficiency; ASLD: argininosuccinate lyase deficiency; CyS: cysteine; GCLC: glutamylcysteine ligase catalytic subunit; GCLM: glutamylcysteine ligase modifier subunit; GS: glutathione synthase; GGT: Gamma-glutamyl transferase; GSH: glutathione; HcyS: homocysteine; MDA: malondialdehyde; OTCD: ornithine transcarbamylase deficiency. Graphs show means ±SD.

Europe PMC Funders Author Manuscripts

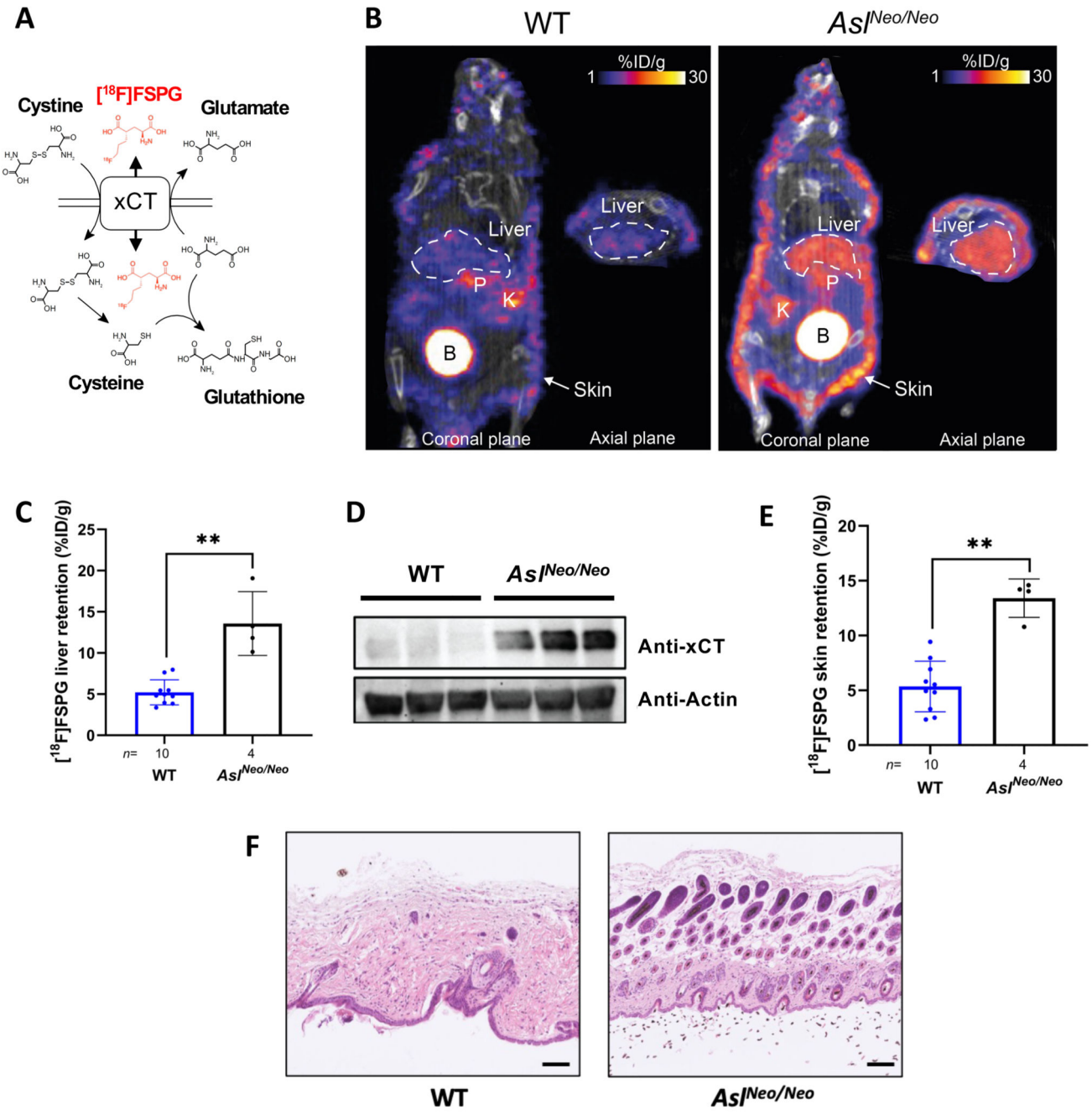

Figure 2. A non-invasive marker confirms the impaired glutathione metabolism in *Asl*$^{Neo/Neo}$ mice.

(A) Schematic overview of system x_c^- function, shuttling cystine, glutamate and [^{18}F]FSPG (red) across the cell membrane. Reduced cystine, cysteine, and glutamate are precursors for glutathione biosynthesis. **(B)** Representative PET/CT images of [^{18}F]FSPG distribution (%ID/g) in the coronal and axial plane of 2 week old WT littermates and *Asl*$^{Neo/Neo}$ mice. P=pancreas, B=bladder, K=kidney. **(C)** Quantified [^{18}F]FSPG retention in the liver 60 min post-injection. **(D)** Western blot of liver xCT expression of WT and *Asl*$^{Neo/Neo}$

mice. **(E)** Quantified [^{18}F]FSPG retention in the skin of WT and *Asl*$^{Neo/Neo}$ mice 60 min post-injection. (**F**) H&E stain from skin of Asl$^{Neo/Neo}$ and WT mice showing architectural differences highlighting the skin abnormality observed in ASL deficiency. Scale bar is 100 μm. (C, E) Unpaired 2-tailed Student's *t* test; **p<0.01. Graphs show mean ±SD.

Europe PMC Funders Author Manuscripts

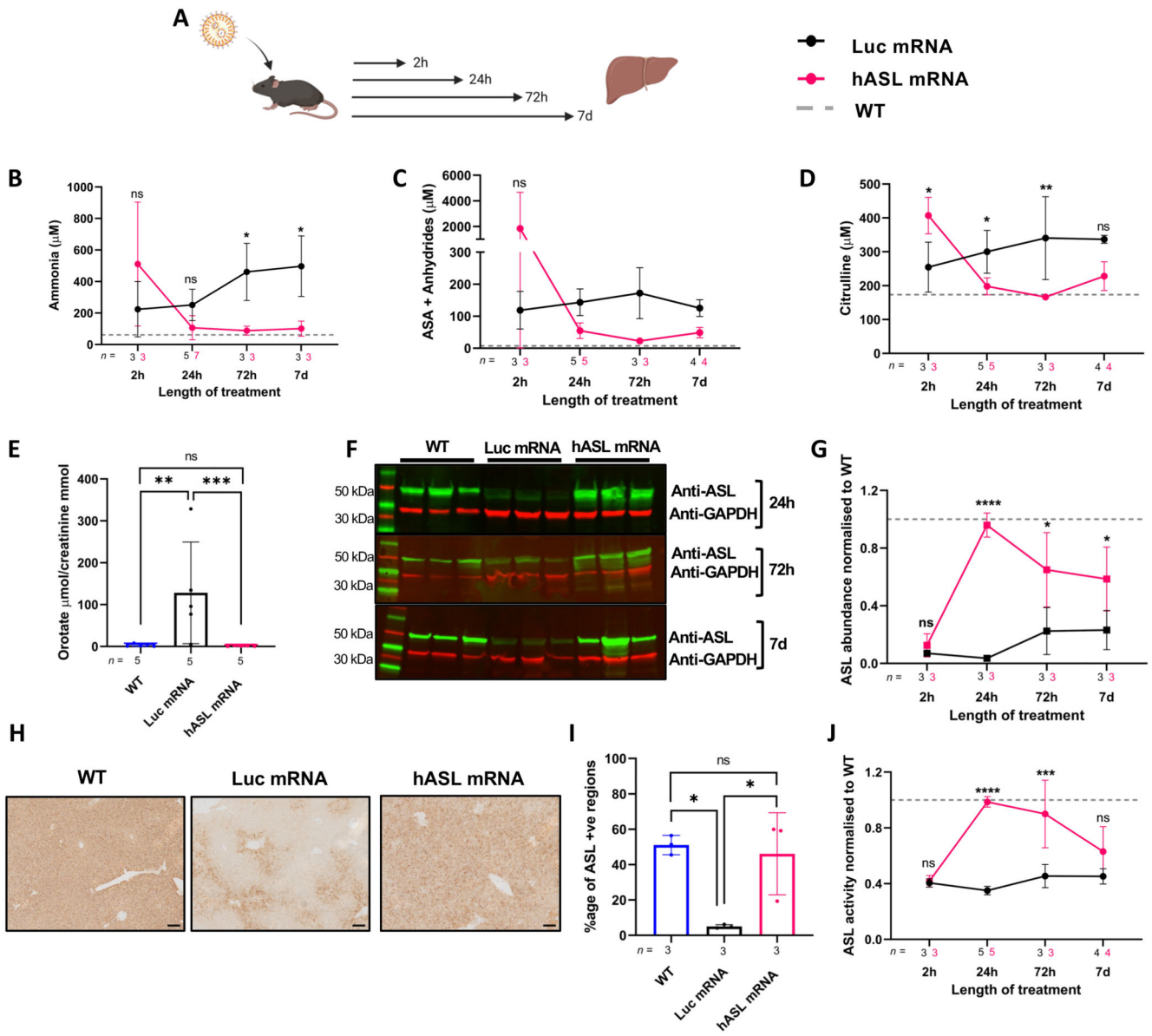

Figure 3. Single intravenous administration of *hASL* mRNA corrects ureagenesis up to 7 days in adult *Asl*$^{Neo/Neo}$ mice

(A) Schematic illustration of experimental plan. Three-week old *Asl*$^{Neo/Neo}$ mice received a single intravenous (IV) injection of either *hASL* or *Luc* mRNA at 1mg/kg body weight and were sacrificed at 2h, 24h, 72h, or 7 days. **(B)** Average ammonia concentrations from plasma and average (**C**) argininosuccinic acid (**D**) citrulline concentrations from dried blood spots at 2, 24, 72 hours, or 7 days. (**E**) Urine orotic acid concentrations normalised to creatinine at 24 hours. (**F**) ASL liver western blot at 24 hours, 72 hours, and 7 days. (**G**) Quantification of ASL immunoblot normalised to GAPDH (**H**) Representative images of liver ASL immunostaining at 24 hours post-mRNA administration and (**I**) Quantification. Scale bar= 100μM. (**J**) Liver ASL activity at 2, 24, 72 hours, and 7 days. Values normalised against WT control. (B, D, G, J) Two-way ANOVA with Šídák's post-hoc test per timepoint.

Grey dotted line represents mean WT values. (C) Two-way ANOVA with Šídák's post-hoc test per timepoint post log transformation, (E) One-way ANOVA post Tukey's post-hoc test comparison post log-transformation (I) One-way ANOVA post Tukey's post-hoc test comparison, ns=not significant, *p<0.05, **p<0.01, ***p<0.005, ****p<0.0001. Graphs show mean ±SD.

Europe PMC Funders Author Manuscripts

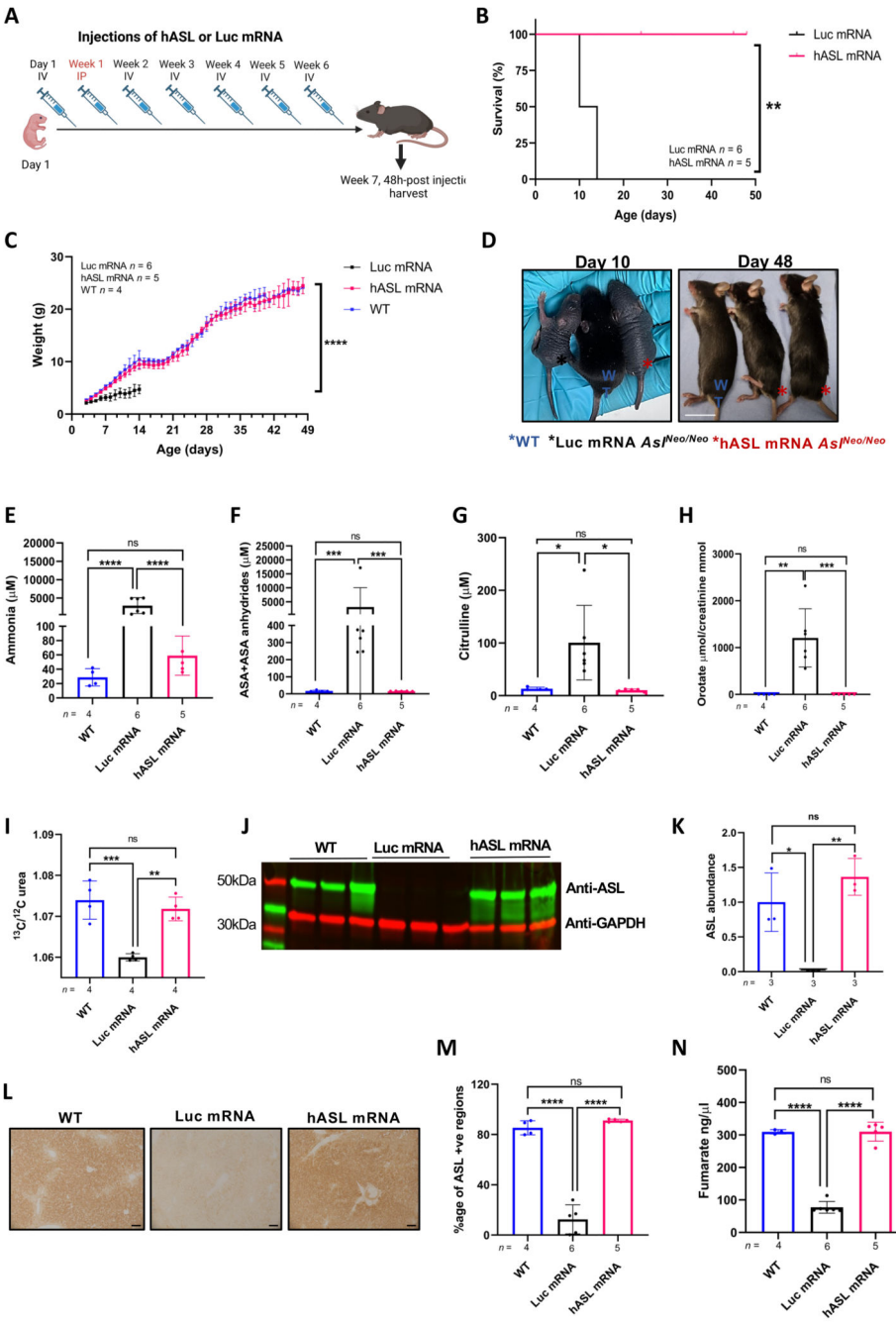

Figure 4. *hASL* mRNA therapy from birth normalises the phenotype of *Asl*$^{Neo/Neo}$ mice.

(**A**) Schematic illustration of experiment. *Asl*$^{Neo/Neo}$ mice were given weekly intravenous (IV) dose of 1mg/kg of either *hASL* or *Luc* mRNA from birth up to 7 weeks, except for week 1 where the mice were administered intraperitoneally with dose of 2 mg/kg. Harvest was performed 48 hours after the last injection. (**B**) Kaplan-Meier survival curve of *hASL*, and *Luc* mRNA-treated *Asl*$^{Neo/Neo}$ mice. (**C**) Average growth curve of WT, *hASL*, and *Luc* mRNA-treated *Asl*$^{Neo/Neo}$ mice. (**D**) Representative images of wild-type (blue asterisk), *hASL* (red asterisk), and *Luc* mRNA-treated (black asterisk) *Asl*$^{Neo/Neo}$ mice at harvest.

Scale bar=2cm. (**E**) Average plasma ammonia, (**F**) argininosuccinic acid (**G**), and citrulline concentrations from dried blood spots, (**H**) urinary orotic acid, and (**I**) C13 ureagenesis from WT, *hASL*, and *Luc* mRNA-treated $Asl^{Neo/Neo}$ mice. (**J**) ASL western blot of WT, *hASL*, and *Luc* mRNA-treated $Asl^{Neo/Neo}$ mice and (**K**) quantification. (**L**) Representative images of ASL immunostaining in livers of WT, *hASL*, and *Luc* mRNA-treated $Asl^{Neo/Neo}$ mice (scale bar=100μM) and (**M**) quantification. (**N**) Liver ASL activity from WT, *hASL*, and *Luc* mRNA-treated $Asl^{Neo/Neo}$ mice livers. (B) Log-rank (Mantel-Cox). (C) Simple linear regression analysis comparing average slopes per group. (E, G-I, K, M, N) One-way ANOVA with Tukey's post-hoc test analysis, (F) One-way ANOVA post Tukey's post-hoc test comparison on log-transformed values, ns=not significant, *p<0.05, **p<0.01, ***p<0.005, ****p<0.0001. Graphs show mean ±SD.

Europe PMC Funders Author Manuscripts

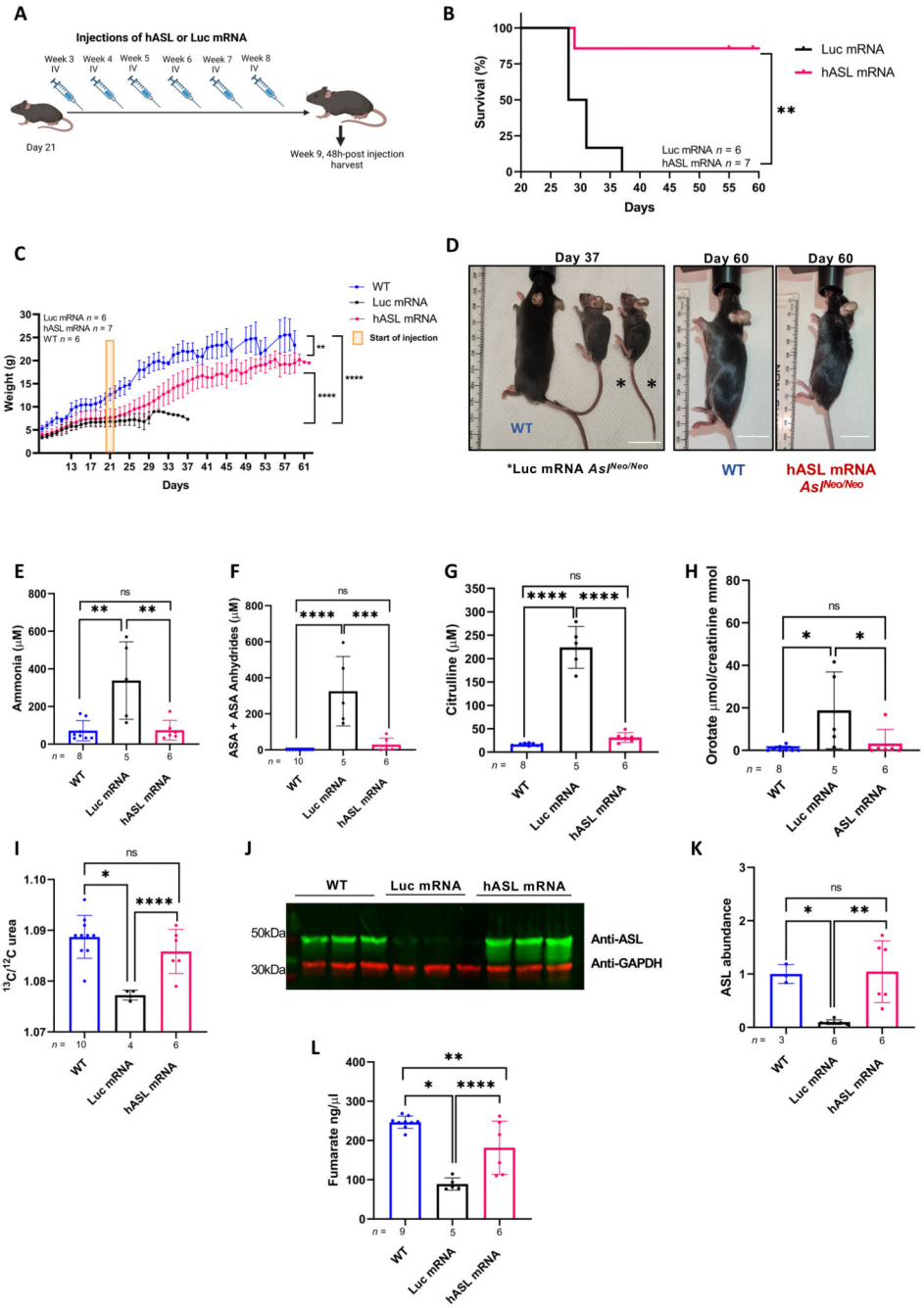

Figure 5. *hASL* mRNA therapy partially rescues the adult phenotype in *Asl*$^{Neo/Neo}$ mice.

(**A**) Schematic illustration of experimental plan. *Asl*$^{Neo/Neo}$ mice were given weekly intravenous (IV) dose of 1mg/kg of either *hASL* or *Luc* mRNA from day 21 up to 9 weeks. (**B**) Kaplan-Meier survival curve of *hASL* and *Luc* mRNA-treated *Asl*$^{Neo/Neo}$ mice. (**C**) Average growth curve of WT, *hASL*, and *Luc* mRNA-treated *Asl*$^{Neo/Neo}$ mice. (**D**) Representative images of WT, *hASL*, and *Luc* mRNA-treated *Asl*$^{Neo/Neo}$ mice at harvest. Scale bar=2cm. (**E**) Average plasma ammonia concentration, (**F**) argininosuccinic acid, (**G**) and citrulline concentrations from dried blood spots, (**H**) urinary orotic acid, and (**I**) C13

ureagenesis from WT, *hASL*, and *Luc* mRNA-treated $Asl^{Neo/Neo}$ mice. (**J**) ASL western blot of WT, *hASL*, and *Luc* mRNA- treated $Asl^{Neo/Neo}$ mice and (**K**) quantification. (**L**) Liver ASL activity from WT, *hASL*, and *Luc* mRNA-treated $Asl^{Neo/Neo}$ mice livers. (B) Log-rank (Mantel-Cox), p=0.0025. (C) Simple linear regression analysis comparing average slopes per group. (F-I, K, L) One-way ANOVA with Tukey's post-hoc test analysis. (E) One-way ANOVA with Tukey's post-hoc test analysis on log-transformed values ns=not significant, *p<0.05, **p<0.01, ****p<0.0001. Graphs show mean ±SD.

Europe PMC Funders Author Manuscripts

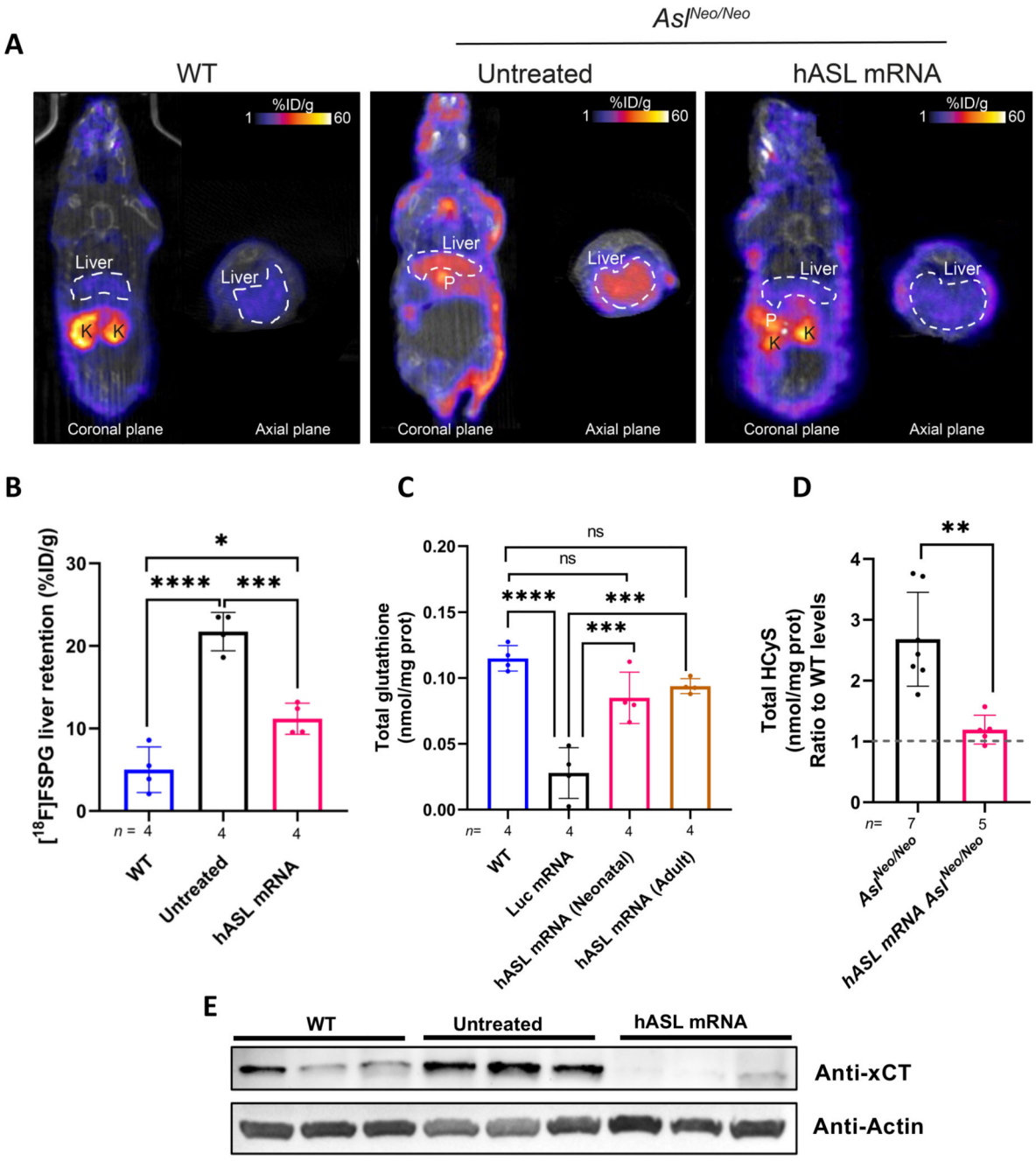

Figure 6. *hASL* mRNA therapy corrects the dysfunction of glutathione metabolism in *Asl*$^{Neo/Neo}$ mice.

(A) [^{18}F]FSPG distribution (%ID/g) in representative coronal and axial plane PET/CT images of WT, untreated *Asl*$^{Neo/Neo}$, and *hASL* mRNA-treated *Asl*$^{Neo/Neo}$ mice. K= Kidney, P= Pancreas. **(B)** [^{18}F]FSPG quantification of the liver in WT, untreated *Asl*$^{Neo/Neo}$, and *hASL* mRNA-treated *Asl*$^{Neo/Neo}$ mice 60 min post-injection. **(C)** Western blot of xCT expression in untreated *Asl*$^{Neo/Neo}$ liver and liver of *hASL* mRNA-treated *Asl*$^{Neo/Neo}$ mice. **(D)** Total glutathione concentrations from liver in WT, Luc mRNA-treated *Asl*$^{Neo/Neo}$ mice,

and *hASL* mRNA-treated *Asl*$^{Neo/Neo}$ mice from neonatal or adulthood. **(E)** Liver total homocysteine concentrations expressed as ratio relative to WT (shown as dotted line) from untreated versus *hASL* mRNA-treated *Asl*$^{Neo/Neo}$ adult mice. Graph shows mean ±SD. (B, D) One-way ANOVA with Tukey's post-hoc test; (E): Unpaired 2-tailed Student's *t* test; ns=not significant, **p<0.01, ***p<0.001, ****p<0.0001.

Europe PMC Funders Author Manuscripts

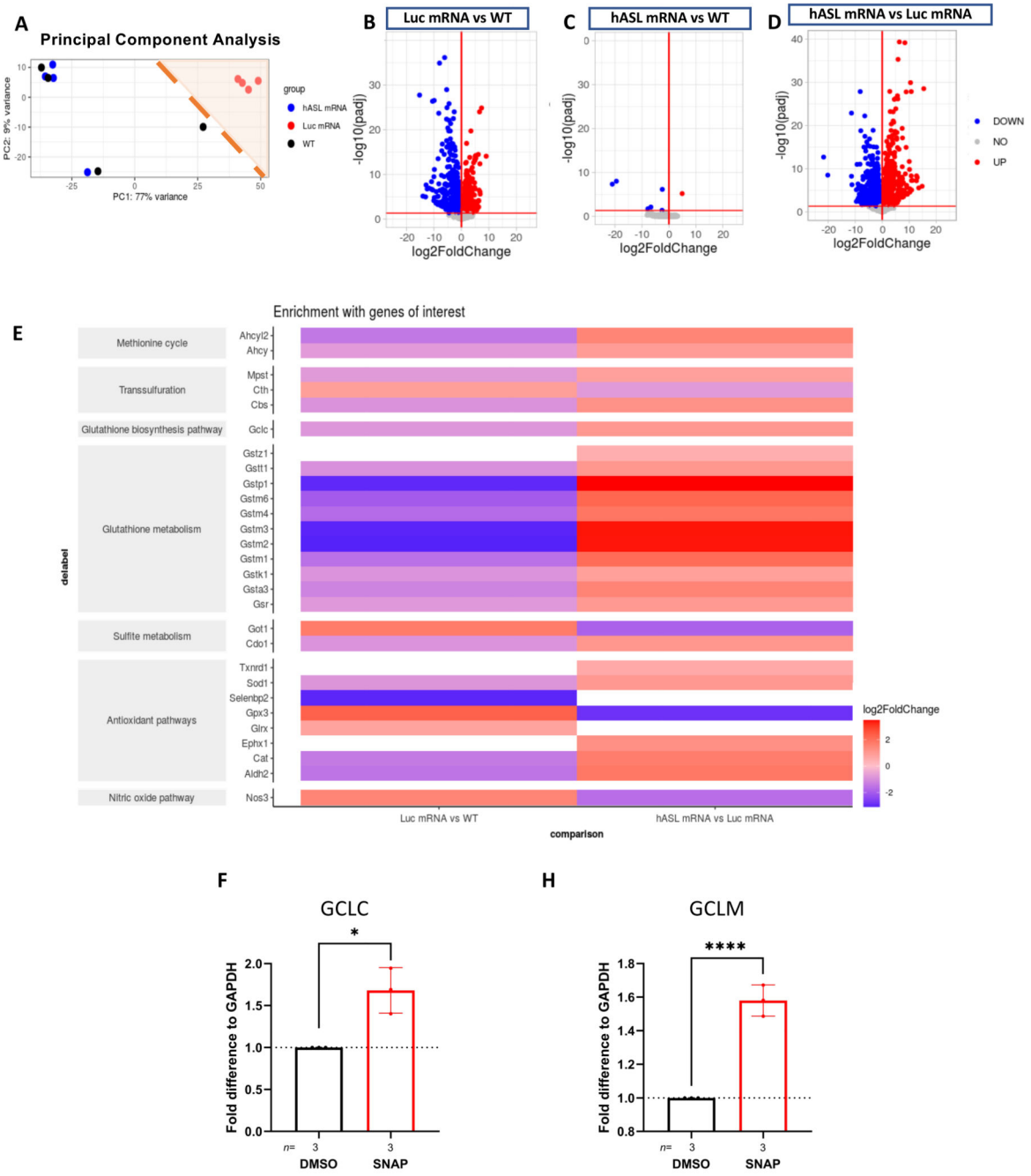

Figure 7. *hASL* mRNA therapy corrects metabolic dysfunction and liver pathophysiology in *Asl*$^{Neo/Neo}$ mice.

(**A**) Principal component analysis plots comparing treatment applied (untreated WT, *hASL* mRNA, or *Luc* mRNA) and mouse genotype (WT or *Asl*$^{Neo/Neo}$) with percentage of variance associated with each axis. (**B**) Volcano plots showing differential gene expression (DEG) analysis of *Luc* mRNA vs WT, (**C**) *hASL* mRNA vs WT, and (**D**) *hASL* mRNA vs *Luc* mRNA. Scatter plots show log-transformed adjusted p-values (<0.05) on the y-axis against log2 fold change (>0.10) values on the x-axis. Blue and red dots represent genes

Europe PMC Funders Author Manuscripts

that were significantly (FDR-corrected p-value of <0.05) downregulated and upregulated, respectively, between groups. Grey dots represent genes that were not significantly altered. (**E**) Pathway analysis highlighting genes of interest significantly altered in DEG analysis organised with their associated pathways when comparing *Luc* mRNA vs WT and *hASL* mRNA vs *Luc* mRNA groups. mRNA expression of **(F)** *GCLC* and **(G)** *GCLM* with NO donor SNAP at 200μM versus control DMSO in Huh7 cells. (**F, G**): Unpaired 2-tailed Student's *t* test; ns=not significant, ***p<0.001, ****p<0.0001; average values from 3 independent experiments. Each dot represents one experiment.

Europe PMC Funders Author Manuscripts